Mismatches between soil and air temperature

Jonas J. Lembrechts[1,*,x], Johan van den Hoogen[2,*], Juha Aalto[3,4], Michael B. Ashcroft[5,6], Pieter De Frenne[7], Julia Kemppinen[8], Martin Kopecký[9,10], Miska Luoto[4], Ilya M. D. Maclean[11], Thomas W. Crowther[2], Joseph J. Bailey[12], Stef Haesen[13], David H. Klinges[14,15], Pekka Niittynen[4], Brett R. Scheffers[16], Koenraad Van Meerbeek[13], Peter Aartsma[17], Otar Abdalaze[18], Mehdi Abedi[19], Rien Aerts[20], Negar Ahmadian[19], Antje Ahrends[21], Juha M. Alatalo[22], Jake M. Alexander[23], Camille Nina Allonsius[24], Jan Altman[9], Christof Ammann[25], Christian Andres[26], Christopher Andrews[27], Jonas Ardö[28], Nicola Arriga[29], Alberto Arzac[30], Valeria Aschero[31,32], Rafael L. Assis[33], Jakob Johann Assmann[34,35], Maaike Y. Bader[36], Khadijeh Bahalkeh[19], Peter Barančok[37], Isabel C. Barrio[38], Agustina Barros[39], Matti Barthel[26], Edmund W. Basham[14], Marijn Bauters[40], Manuele Bazzichetto[41], Luca Belelli Marchesini[42], Michael C. Bell[43], Juan C. Benavides[44], José Luis Benito Alonso[45], Bernd J. Berauer[46,47], Jarle W. Bjerke[48], Robert G. Björk[49,50], Mats P. Björkman[49,50], Katrin Björnsdóttir[51], Benjamin Blonder[52], Pascal Boeckx[40], Julia Boike[53,54], Stef Bokhorst[20], Bárbara N. S. Brum[55], Josef Brůna[9], Nina Buchmann[56], Pauline Buysse[57], José Luís Camargo[58], Otávio C. Campoe[59], Onur Candan[60], Rafaella Canessa[36], Nicoletta Cannone[61], Michele Carbognani[62], Jofre Carnicer[63,64], Angélica Casanova-Katny[65], Simone Cesarz[66,67], Bogdan Chojnicki[68,68], Philippe Choler[69,70], Steven L. Chown[71], Edgar F. Cifuentes[72], Marek Čiliak[73], Tamara Contador[74,75], Peter Convey[76], Elisabeth J. Cooper[77], Edoardo Cremonese[78], Salvatore R. Curasi[79], Robin Curtis[11], Maurizio Cutini[80], C. Johan Dahlberg[81,82], Gergana N. Daskalova[83], Miguel Angel de Pablo[84], Stefano Della Chiesa[85], Jürgen Dengler[86,87,66], Bart Deronde[88], Patrice Descombes[89], Valter Di Cecco[90], Michele Di Musciano[91], Jan Dick[27], Romina D. Dimarco[92], Jiri Dolezal[9,93], Ellen Dorrepaal[94], Jiří Dušek[95], Nico Eisenhauer[66,67], Hamid Ejtehadi[96], Lars Eklundh[28], Mohammad Bagher Erfanian[96], Todd E. Erickson[97,98], Brigitta Erschbamer[99], Werner Eugster[26], Robert M. Ewers[100], Dan A. Exton[101], Nicolas Fanin[102], Fatih Fazlioglu[60], Iris Feigenwinter[26], Giuseppe Fenu[103], Olga Ferlian[66,67], M. Rosa Fernández Calzado[104], Eduardo Fernández-Pascual[105], Manfred Finckh[106], Rebecca Finger Higgens[107], T'ai G. W. Forte[62], Erika C. Freeman[108], Esther R. Frei[109,110], Eduardo Fuentes-Lillo[111,1,112], Rafael A. García[111,113], María B. García[114], Charly Géron[115], Mana Gharun[26], Dany Ghosn[116], Khatuna Gigauri[117], Anne Gobin[118,119], Ignacio Goded[29], Mathias Goeckede[120], Felix Gottschall[66,67], Keith Goulding[121], Sanne Govaert[7], Bente Jessen Graae[122], Sarah Greenwood[123], Caroline Greiser[81], Achim Grelle[124], Benoit Guénard[125], Mauro Guglielmin[126], Joannès Guillemot[127,128], Peter Haase[129,130], Sylvia Haider[131,66], Aud H. Halbritter[132], Maroof Hamid[133], Albin Hammerle[134], Arndt Hampe[135], Siri V. Haugum[132], Lucia Hederová[9], Bernard Heinesch[136], Carole Helfter[137], Daniel Hepenstrick[86], Maximiliane Herberich[138], Mathias Herbst[139], Luise Hermanutz[140], David S. Hik[141], Raúl Hoffrén[142], Jürgen Homeier[143], Lukas Hörtnagl[56], Toke T. Høye[144], Filip Hrbacek[145], Kristoffer Hylander[81], Hiroki Iwata[146], Marcin Antoni Jackowicz-Korczynski[147,28], Hervé Jactel[148], Järvi Järveoja[149], Janusz Olejnik[150], Szymon Jastrzębowski[151], Anke Jentsch[47,152], Juan J. Jimenez[153,154], Ingibjörg S. Jónsdóttir[155], José João L. L. Souza[156], Tommaso Jucker[157], Alistair S. Jump[158], Radoslaw Juszczak[68], Róbert Kanka[37], Vít Kašpar[9,159], George Kazakis[116], Julia Kelly[160], Anzar A. Khuroo[133], Leif Klemedtsson[49], Marcin Klisz[151], Natascha Kljun[160], Alexander Knohl[161], Johannes Kobler[162], Jozef Kollár[37], Martyna M. Kotowska[143], Bence Kovács[163], Juergen Kreyling[164], Andrea Lamprecht[165], Simone I. Lang[166], Christian Larson[167], Keith Larson[168], Kamil Laska[145,169], Guerric le Maire[127,128], Rachel I. Leihy[71], Luc Lens[170], Bengt Liljebladh[49], Annalea Lohila[171,172], Juan Lorite[104,173], Benjamin Loubet[57], Joshua Lynn[132], Martin Macek[9], Roy Mackenzie[74], Enzo Magliulo[174], Regine Maier[26], Francesco Malfasi[61], František Máliš[175], Matěj Man[9], Giovanni Manca[29], Antonio Manco[176], Tanguy Manise[136], Paraskevi Manolaki[177,178,179], Felipe Marciniak[55], Marianna Nardino[180], Radim Matula[10,181], Ana Clara Mazzolari[32], Sergiy Medinets[182], Volodymyr Medinets[182], Camille Meeussen[7], Sonia Merinero[81], Rita de Cássia Guimarães Mesquita[183], Katrin Meusburger[184], Filip J. R. Meysman[185], Sean T. Michaletz[186], Ann Milbau[187], Dmitry Moiseev[188], Pavel Moiseev[188], Andrea Mondoni[189], Leonardo Montagnani[190], Mikel Moriana-Armendariz[77], Umberto Morra di Cella[191], Martin Mörsdorf[192], Jonathan R. Mosedale[193], Lena Muffler[143], Miriam Muñoz-Rojas[194,97], Jonathan A. Myers[195], Isla H. Myers-Smith[83], Laszlo Nagy[196], Ilona Naujokaitis-Lewis[197], Lena Nicklas[99], Georg Niedrist[85], Armin Niessner[198], Mats B. Nilsson[149], Signe Normand[34,35], Marcelo D. Nosetto[199,200], Yann Nouvellon[127,128], Martin A. Nuñez[201], Romà Ogaya[202,64], Jérôme Ogée[102], Joseph Okello[40,203,204], Jørgen Eivind Olesen[205], Øystein Opedal[206], Simone Orsenigo[207], Andrej Palaj[37], Timo Pampuch[208], Alexey V. Panov[209], Meelis Pärtel[210], Ada Pastor[211,178], Aníbal Pauchard[111,113], Harald Pauli[165], Marian Pavelka[95], William D. Pearse[212,213], Matthias Peichl[149], Loïc Pellissier[214,215], Rachel M. Penczykowski[216], Josep Penuelas[202,64], Matteo Petit Bon[166,77,217], Alessandro Petraglia[62], Shyam S. Phartyal[218], Gareth K. Phoenix[219], Casimiro Pio[220], Andrea Pitacco[221], Camille Pitteloud[214,215], Roman Plichta[181], Francesco Porro[189], Miguel Portillo-Estrada[1], Jérôme Poulenard[222], Poyatos Poyatos[64,223], Anatoly S. Prokushkin[209,30], Radoslaw Puchalka[224,225], Mihai Pușcaș[226,227,228], Dajana Radujković[1], Krystal Randall[229], Amanda Ratier Backes[131,66], Sabine Remmele[198], Wolfram Remmers[230], David Renault[41,231], Anita C. Risch[232], Christian Rixen[109], Bjorn J.M.

Robroek[233], Adrian V. Rocha[234], Christian Rossi[235,236], Graziano Rossi[189], Olivier Roupsard[237,238,239], Alexey V. Rubtsov[30], Clotilde Sagot[240], Jhonatan Sallo Bravo[241,242], Cinthya C. Santos[243], Judith M. Sarneel[244], Tobias Scharnweber[208], Jonas Schmeddes[164], Marius Schmidt[245], Thomas Scholten[246], Naomi Schwartz[247], Tony Scott[121], Julia Seeber[85,248], Ana Cristina Segalin de Andrade[243], Tim Seipel[167], Philipp R. Semenchuk[249], Rebecca A. Senior[250], Josep M. Serra-Diaz[251], Piotr Sewerniak[252], Ankit Shekhar[56], Nikita V. Sidenko[209], Lukas Siebicke[161], Laura Siegwart Collier[140,253], Elizabeth Simpson[212], David Siqueira[254], Zuzana Sitková[255], Johan Six[26], Marko Smiljanic[208], Stuart W. Smith[122,256], Sarah Smith-Tripp[257], Ben Somers[258], Mia Vedel Sørensen[122], Bartolomeu Israel Souza[259], Arildo Souza Dias[260,243], Marko J. Spasojevic[261], James D. M. Speed[262], Fabien Spicher[263], Angela Stanisci[264], Klaus Steinbauer[165], Rainer Steinbrecher[265], Michael Steinwandter[85], Michael Stemkovski[212], Jörg G. Stephan[266], Christian Stiegler[161], Stefan Stoll[230,267], Martin Svátek[181], Miroslav Svoboda[10], Torbern Tagesson[28,268], Andrew J. Tanentzap[108], Franziska Tanneberger[269], Jean-Paul Theurillat[270,271], Haydn J. D. Thomas[83], Andrew D. Thomas[272], Katja Tielbörger[273], Marcello Tomaselli[62], Urs Albert Treier[34,35], Mario Trouillier[208], Pavel Dan Turtureanu[226,274,228], Rosamond Tutton[275], Vilna A. Tyystjärvi[4,3], Masahito Ueyama[276], Karol Ujházy[175], Mariana Ujházyová[73], Domas Uogintas[277], Anastasiya Vladimirovna Urban[209,181], Josef Urban[181,30], Marek Urbaniak[150], Tudor-Mihai Ursu[278], Francesco Primo Vaccari[279], Stijn Van de Vondel[280], Liesbeth van den Brink[273], Maarten Van Geel[281], Vigdis Vandvik[132], Pieter Vangansbeke[7], Andrej Varlagin[282], G.F. Ciska Veen[283], Elmar Veenendaal[284], Susanna E. Venn[285], Hans Verbeeck[286], Erik Verbrugggen[1], Frank G.A. Verheijen[287], Luis Villar[288], Luca Vitale[289], Pascal Vittoz[290], Maria Vives-Ingla[64], Jonathan von Oppen[34,35], Josefine Walz[94], Runxi Wang[125], Yifeng Wang[275], Robert G. Way[275], Ronja E. M. Wedegärtner[122], Robert Weigel[143], Jan Wild[9,159], Matthew Wilkinson[43], Martin Wilmking[208], Lisa Wingate[102], Manuela Winkler[165], Sonja Wipf[235], Georg Wohlfahrt[134], Georgios Xenakis[291], Yan Yang[292], Zicheng Yu[293,294], Kailiang Yu[295], Florian Zellweger[110], Jian Zhang[296,297], Zhaochen Zhang[296], Peng Zhao[149], Klaudia Ziemblińska[150], Reiner Zimmermann[198,298], Shengwei Zong[299], Viacheslav I. Zyryanov[209], Ivan Nijs[1,+], Jonathan Lenoir[263,+,x]

* These authors contributed equally to this work

[x] Corresponding authors: Jonas.lembrechts@uantwerpen.be, jonathan.lenoir@u-picardie.fr

[+] These authors contributed equally to this work

** See end of manuscript for affiliations

Summary paragraph

Research in environmental science relies heavily on global climatic grids derived from estimates of air temperature at around 2 meter above ground[1-3]. These climatic grids however fail to reflect conditions near and below the soil surface, where critical ecosystem functions such as soil carbon storage are controlled and most biodiversity resides[4-8]. By using soil temperature time series from over 8500 locations across all of the world's terrestrial biomes[4], we derived global maps of soil temperature-related variables at 1 km resolution for the 0–5 and 5–15 cm depth horizons. Based on these maps, we show that mean annual soil temperature differs markedly from the corresponding 2 m gridded air temperature, by up to 10°C, with substantial variation across biomes and seasons. Soils in cold and/or dry biomes are annually substantially warmer (3.6°C ± 2.3°C) than gridded air temperature, whereas soils in warm and humid environments are slightly cooler (0.7 ± 2.3°C). As a result, annual soil temperature varies less (by 17%) across the globe than air temperature. The effect of macroclimatic conditions on the difference between soil and air temperature highlights the importance of considering that macroclimate warming may not result in the same level of soil temperature warming. Similarly, changes in precipitation could alter the relationship between soil and air temperature, with implications for soil-atmosphere feedbacks[9]. Our results underpin that the impacts of climate and climate change on biodiversity and ecosystem functioning are inaccurately assessed when air rather than soil temperature is used, especially in cold environments.

Main

With rapidly increasing availability of big data on species distributions, functional traits and ecosystem functioning[10-13], we can now study biodiversity and ecosystem responses to global change in unprecedented detail[2,3,14,15]. Temperature plays a central role in mediating ecological, physiological, biophysical and biogeochemical processes, numerous spatially-explicit studies across a wide range of disciplines make use of global gridded temperature data[2,16,17]. However, these data sets use measurements from standard meteorological stations that record air temperature inside well-ventilated protective shields placed up to 2 m above-ground in open, shade-free habitats[4,18]. Such conditions seldom reflect the climatic conditions near or below the soil surface that most organisms experience, and where important ecosystem functions and processes operate[5,19,20]. This mismatch or offset between soil and air temperature can easily reach up to ±10°C annually[7,21,22].

The direction and magnitude of the mismatch between soil and air temperature is largely driven by energy balances (e.g., evaporation and incoming and outgoing radiation mediated by wind), by the insulating effects of snow and by vegetation characteristics (e.g., canopy cover, height, and functional traits related to light reflectance and stomatal conductance), and soil characteristics (e.g., latent heat and specific heat capacity, dependent on soil type and texture as well as water content)[4,7,23-26]. The factors implicated in soil-air temperature offsets do not only vary spatially, but also seasonally[7,27], and in predictable and different ways across macroclimatic gradients. We therefore expect biome-wide patterns in seasonal and annual variation in offsets.

Several ecological patterns and processes relate more directly to soil temperature than to air temperature. Soil rather than air temperatures better predict ecosystem functions like biogeochemical cycling (e.g., organic matter decomposition, soil respiration or the global aspects of the carbon balance)[28-33]. Similarly, the use of soil temperature in correlative analyses or predictive models may improve predictions of climate impacts on organismal physiology, behaviour, and population and community dynamics[8,33-37]. Given the key role of soil-related processes for both above- and belowground parts of the ecosystem and their feedbacks to the atmosphere[38], adequate soil temperature data are of critical importance for a broad range of fields of study, such as ecology, biogeography, agronomy, soil science and climate system dynamics.

In response to the challenges outlined above, we used over 8,500 time series of soil temperature measured *in-situ* between 1979 and 2020 (mean duration 2.8 years, ranging from 1 month to 41 years), from across the world's major terrestrial biomes, compiled in the SoilTemp database[4] (Fig. 1a, Extended data Fig. 1). First, we assessed the global and biome-specific patterns in the mean annual offset between *in situ* soil temperature (topsoil: 0–5 cm and second layer: 5–15 cm depth) and coarse-scale interpolated air temperature from ERA5-Land (soil temperature minus air temperature, hereafter called the *temperature offset, sensu De Frenne, et al.* [39]). Next, we used a machine learning approach with 31 environmental explanatory variables (namely climate, soil, topography, reflectance, vegetation and anthropogenic variables) to model the spatial variation in monthly temperature offsets at a 1 x 1 km resolution for all continents except Antarctica (see Methods). Using these offsets, we then calculated relevant soil-related bioclimatic variables (SBIO) and assessed patterns in mean annual soil temperature across the world's biomes. Comparing the latter with mean annual air temperature across the biomes helps to quantify the strength and direction of the relationships between soil and air temperature across space and time with the potential to improve our understanding of land-atmosphere feedbacks[9].

Biome-wide patterns in the temperature offset

We found temperature offsets between *in situ* measured mean annual topsoil and air temperature of up to 10°C (Fig. 1, 0–5 cm depth, averaged at 1-km² resolution, 5–15 cm is available in Extended data Figs. 2-3); the values are in line with data from regional studies[7,22,27]. The magnitude and direction of these offsets varied considerably within and across biomes. Mean annual topsoil temperature was on average 3.6 ± 2.3°C higher than air temperature in cold and/or dry biomes, namely tundra, boreal forests, temperate grasslands and subtropical deserts. In contrast, offsets were slightly negative in warm and wet biomes, namely in tropical savannas, temperate forests and tropical rain forests, where on average soils were 0.7 ± 2.7°C cooler than air (Fig. 1b, Extended data Figs. 2 and 3; note, however, the lower spatial coverage in these biomes in Fig. 1a, c, d, Extended data Table 1). Temperature offsets in annual minimum and maximum temperature (5^{th} and 95^{th} percentile, see Methods) amounted to c. 10°C. While annual soil temperature minima were on average higher than corresponding air temperature minima in all biomes, temperature offsets of annual maxima followed largely the same biome-related trends as seen for the annual means, albeit with the highest variability expected for temperature extremes (Extended data Figs. 2g, h, 3g, h). This clear discrepancy between cold and dry versus warm and wet biomes indicates the known decoupling resulting from snow (from cold extremes in cold and cool biomes) and buffering due to shading, evaporation and the specific heat of water (mostly against warm extremes in warm and wet biomes) for soil temperatures[7,26,40-44]. As such, these results highlight strong macroclimatic impacts on microclimate across the globe. Using different air temperature data sources did not alter the annual temperature offset and biome-related patterns (see Methods and Extended data Figs. 2-5).

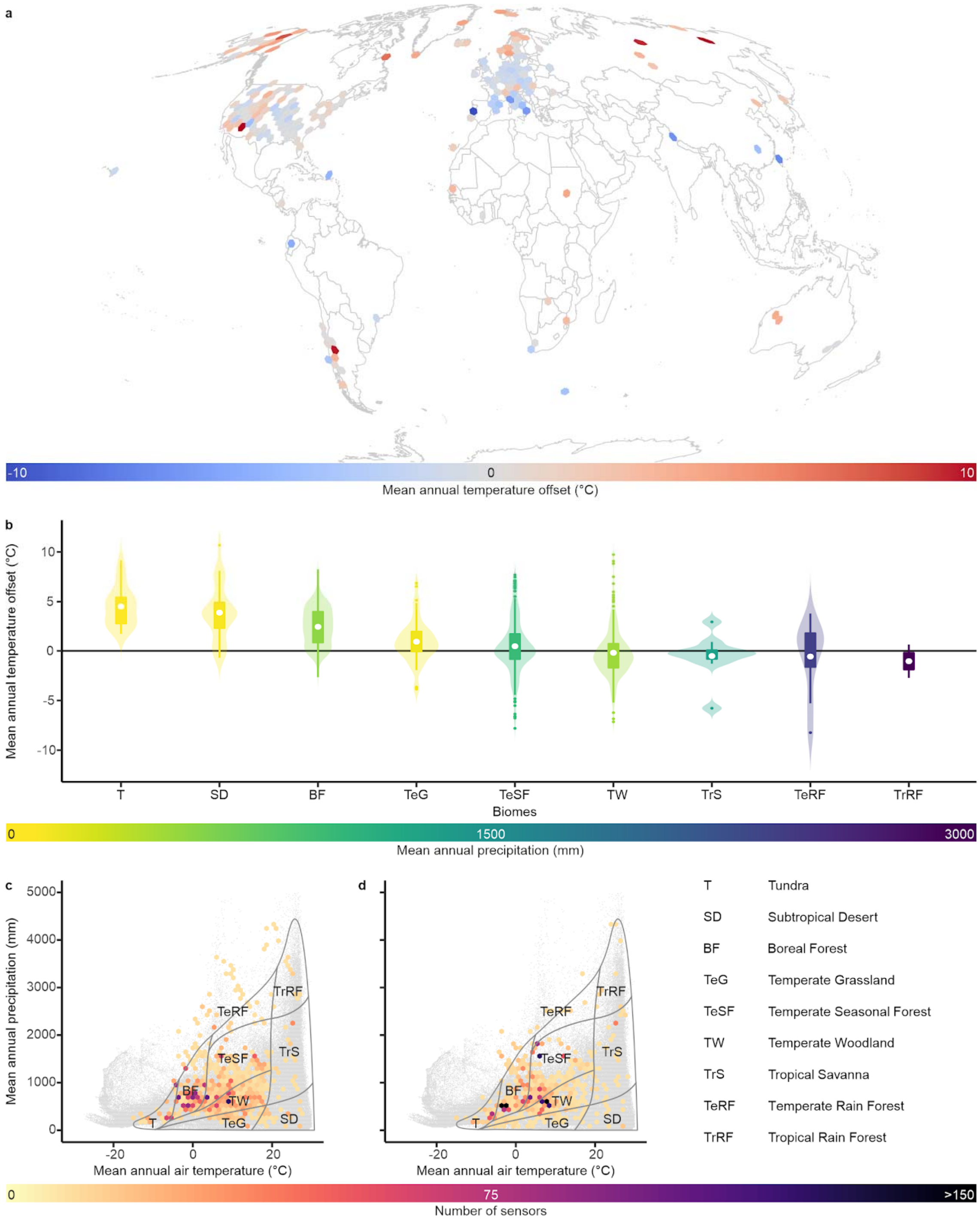

Figure 1: Temperature offsets between soil and air temperature differ significantly between biomes. *(a) Distribution of in situ measurement locations across the globe, coloured by the mean annual temperature offset (in °C) between in situ measured soil temperature (topsoil, 0–5 cm depth) and modelled interpolated weather-station based air temperature. Offsets were averaged per hexagon, each with a resolution of approximately 70,000 km². Mollweide projection. (b) Mean annual temperature offsets per Whittaker biome (adapted from Whittaker 1970, based on*

geographic location of sensors averaged at 1 km²; 0–5 cm depth), ordered by mean temperature offset and coloured by mean annual precipitation. (c–d) Distribution of sensors in 2D climate space for the topsoil (c, 0–5 cm depth, N=4530) and the second layer (d, 5–15 cm depth, N=3989). Colours of hexagons indicate the number of sensors at each climatic location, with a 40 × 40 km resolution. Grey dots in the background represent the global variation in climatic space (obtained by sampling 1,000,000 random locations from the CHELSA world maps). Overlay with dotted lines depicts a delineation of Whittaker biomes.

Temporal and spatial variation in temperature offsets

We found a strong seasonality in monthly temperature offsets, especially towards higher latitudes (Fig. 2), using a random forest (RF, so called as it is made up of many decision trees) modelling approach[2]. This model paired the monthly temperature offsets with 31 global gridded (1 km²) covariate layers of climate, soil, topography, reflectance, vegetation and anthropogenic variables (Supplementary Table 1) and interpolated these offsets across the biomes. High-latitude soils were found to be several degrees warmer than the air (monthly offsets of up to 25°C) during their respective winter months, and cooler (up to 10°C) in summer months, both at 0–5 cm and at 5–15 cm depths (Fig. 2, Extended data Fig. 6). In the tropics and subtropics, soils in dry biomes (e.g., the Sahara desert or southern Africa) were predicted to be warmer than air throughout most of the year, whilst soils in mesic biomes (e.g., tropical biomes in South America, central Africa and Southeast Asia) were modelled to be consistently cooler than air temperature throughout the year in both soil layers[9]. This seasonal variation is in line with the annual differences observed above, and highlights even more strongly the likely role of snow and soil moisture[7,26,40-44].

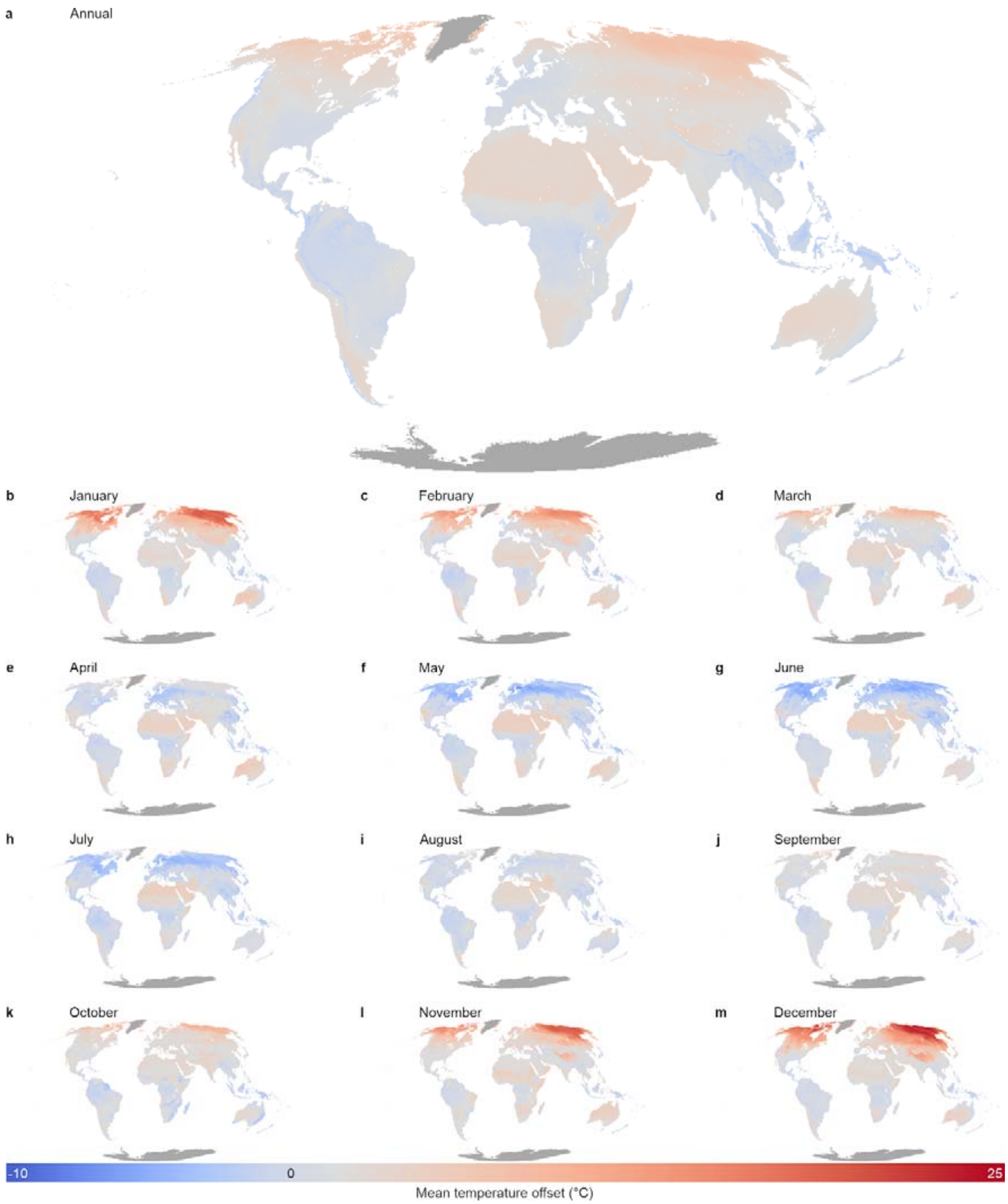

Figure 2: Global modelled temperature offsets between soil and air temperature show strong spatiotemporal variation across months. *Modelled annual (a) and monthly (b–m) temperature offset (in °C) between in situ measured soil temperature (topsoil, 0–5 cm) and modelled air temperature. Positive (red) values indicate soils that are warmer than the air. Dark grey represents regions outside the modelling area.*

Our bootstrap approach to validate our modelled offsets indicated high consistency among the outcomes of 100 bootstrapped models (Fig. 3, Extended data Fig. 7a), with standard deviations in most months and across most parts of the globe around or below ±1°C. One exception to this was the temperature offset at high latitudes of the northern hemisphere during winter months (standard deviation up to ±5°C in the 0–5 cm layer). There, high variation in the *in situ* measured offsets – likely driven by the interactions between snow, local topography and vegetation – reduced predictive power of the models at 1-km² resolution[25,42,45-47]. In the coldest and warmest extremes of the temperature gradient, our model predictions underestimated measured temperature offsets by around 1°C (Extended data Fig. 8). Predictive performance was comparable across biomes, although with large variation in data availability (Extended data Fig. 9).

The importance of explanatory variables in the RF models was largely consistent across months. Macroclimatic variables such as incoming solar radiation, air temperature and precipitation were by far the most influential explanatory variables in the spatial models of the monthly temperature offset (Extended data Figs. 10, 11). The offset had a strong negative covariation with both air temperature and solar radiation, strengthening our conclusion that the overarching global patterns in the temperature offset might indeed be mostly driven by the opposing processes at play in cool (decoupling effects of snow) versus warm (buffering effects of soil moisture) biomes. Importantly, however, snow cover itself was not a good predictor of the temperature offset in most months (except for January and December), likely due to fine-scale variation in snow depth and its insulating properties below the studied 1-km² resolution[25,48,49]. The secondary importance of variables related to precipitation and soil structure hints to the additional distinction between wet and dry biomes at the warm end of the temperature gradient, where landscapes with wet soils and the presence of closed-canopy vegetation generally have cooler soils as the heating and evaporating of soil moisture absorbs significant portions of the energy, a process much less at play in warm and dry biomes[9,43,45] (Extended data Fig. 11).

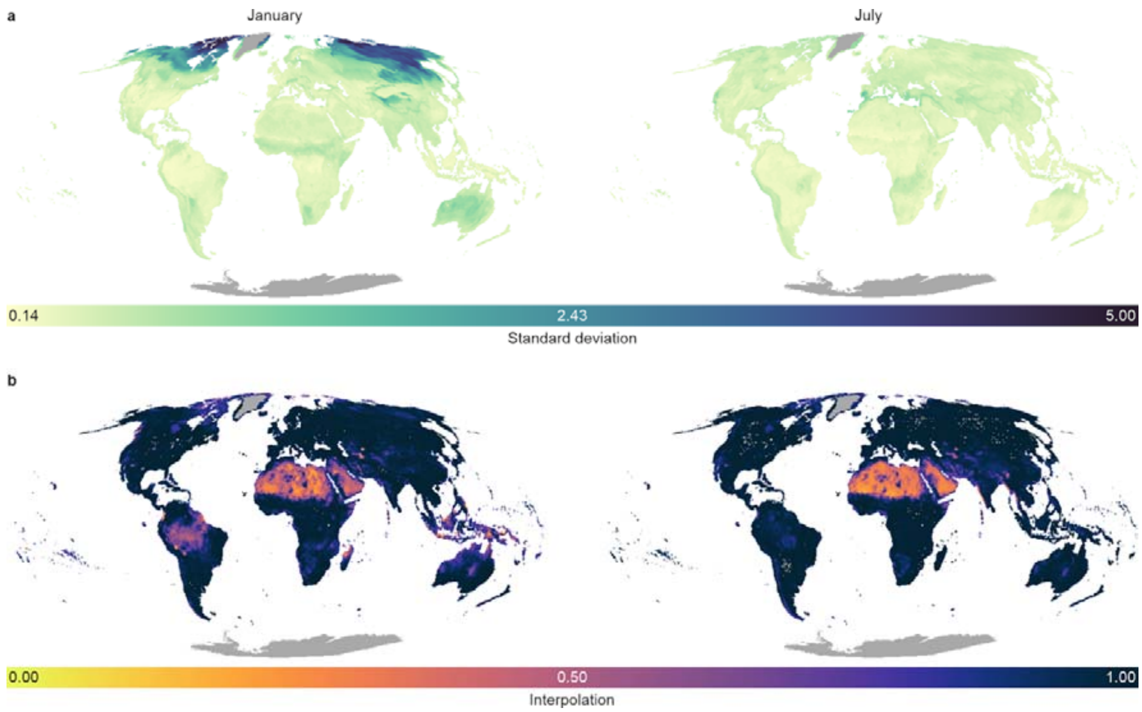

Figure 3: Models of the temperature offset between soil and air temperature have low standard deviations and good global coverage. *Analyses for the temperature offset between in situ topsoil (0–5 cm depth) temperature and gridded air temperature. (a) Standard deviation (in °C) over the predictions from a cross-validation analysis that iteratively varied the set of covariates (explanatory data layers) and model hyperparameters (see Methods for details) across 100 models and evaluated model strength using 10-fold cross-validation, for January (left) and July (right), as examples of the two most contrasting months. (b) The fraction of axes in the multidimensional environmental space for which the pixel lies inside the range of data covered by the sensors in the database. Low values indicate increased extrapolation.*

Our empirical modelling approach enabled us to map global patterns in soil temperature. In doing so, we did not necessarily disentangle the mechanisms driving the temperature offset, which would require modelling the biophysics of energy exchange at the soil surface across biomes[50,51]. Indeed, many of the strongest explanatory variables used in our study (e.g., macroclimate, and especially the negative correlation of the temperature offset with solar radiation input) are related to the identified temperature offset more indirectly than directly. Importantly, however, these macroclimatic variables initiate many factors downstream that affect the functioning of ecosystems at fine spatial scales which, in turn, feedback on the local offset, such as energy and water balances, snow cover, wind intensity and vegetation cover. For example, while increased solar radiation itself would result in warmer soils than the air, high solar radiation at the global scale often coincides with high vegetation cover, which results in cooler soils[39]. These results highlight, however, that the complex relationship between microclimatic soil temperature and macroclimatic air temperature is predictable across macroclimatic gradients, even when governed by a multitude of factors at higher resolutions.

We used a 1 × 1 km resolution to model mismatches between soil and temperature, however, higher resolutions could reveal the importance of locally heterogenous variables. These variables include micro-topography (e.g., slope and topographic roughness), vegetation characteristics (e.g., biomass and structure), land use, soil moisture and snow cover would emerge among the most important drivers at higher spatiotemporal resolutions than used here, even though they seem secondary at 1 × 1 km resolution (Extended data Fig. 10). Indeed, we averaged all values from different microhabitats (e.g., sensors in forested versus open patches within 1 × 1 km grid cells) to obtain overarching patterns, as well as all daily and diurnal variation within a month, even though important variation is, no doubt, present at high resolutions. For example, we show that soils in the temperate seasonal forest biome were on average 0.5°C warmer annually than air temperatures, while they were 0.8°C cooler than the air in forested habitats, and 1°C warmer than the air in non-forested habitats (Extended data Table 2). The incorporation of factors that affect the local radiation balance and wind (e.g., topography, vegetation cover, urbanization) at the landscape to local scales will be critical when predicting soil temperature at higher spatiotemporal resolutions. Similarly, it is likely to be important to integrate horizontal mechanistic processes in specific microhabitats, such as the effects of neighbouring locations (e.g. topographic shading and cold-air drainage, [4,52,53]). The SoilTemp database[4], with its georeferenced time series of *in situ* measured soil and near-surface temperature and associated metadata, can facilitate the necessary steps towards higher resolutions to be taken in the future.

Although the over-representation of some biomes was accounted for in the modelling by averaging the data at 1 × 1 km resolution, geographic bias is present as in most global databases, and some areas still contained an insufficient amount of field observations to be well represented. For 18% of pixels across the biomes, less than 90% of environmental variables fell within the range covered by the database. Our global maps should therefore be used with caution in regions where environmental conditions are outside the range of our sampled data. The current availability of microclimatic data are indeed significantly fewer in tropics (Extended data Table 3). There, our model has extrapolated temperature values beyond the range used to calibrate the model in some cases (Fig. 3b, Extended data Fig. 7b). Our open-access uncertainty estimations (Fig. 3, Extended data Fig. 7) could be used as a mask to exclude areas of model extrapolation (i.e., values of interpolation in Fig. 3b < 0.9), as exemplified in Fig. 4a. Importantly, these same maps identify regions where installation of soil microclimate networks need to be prioritized[4].

Global variation in soil temperature

Using the modelled temperature offsets, we constructed soil-related analogues of temperature-derived bioclimatic variables (SBIO 1-11, Fig. 4, Extended data Figs. 12, 13) by adding monthly and annual temperature offsets to the original air-temperature based bioclimatic variables of the CHELSA database[1]. The latter, calculated by summarizing the monthly mean, minimum and maximum temperature values over the period 1979–2013, are specifically developed for ecological applications and represent annual averages (e.g., mean annual temperature), seasonality (e.g., annual range in temperature), and extreme conditions (e.g., temperatures of the coldest and warmest months).

Our results indicate 17% less spatial variation globally (expressed by the standard deviation) in mean annual soil temperature than in air temperature, largely driven by the positive offset between soil and air temperature in cold environments (Fig. 4). Importantly, our machine learning models slightly underestimate temperature offsets at both extremes of the temperature gradient (Extended data Fig. 8), and estimates of the reduction in variation across space in the coldest biomes are thus conservative. The reduction in spatial temperature variation is observed in all cold and cool biomes, with tundra and boreal forests having both a significant positive mean temperature offset and a reduction of 20% and 22% in variation, respectively (Fig. 4c). In the warmest biomes, however, we see an increase in variation of, on average, 10%. The reduction in variation in cold and cool biomes likely links back to the decoupling effect of snow, while in warm biomes the difference between dry (positive temperature offset) and wet (negative temperature offset) environments could cause increased variation. The well-supported decoupling effect of soils suggests that soil-related organisms in cold biomes are exposed to a narrower temperature range relative to organisms operating in free-air conditions, implying a potentially higher climate-sensitivity to the same level of climate warming.

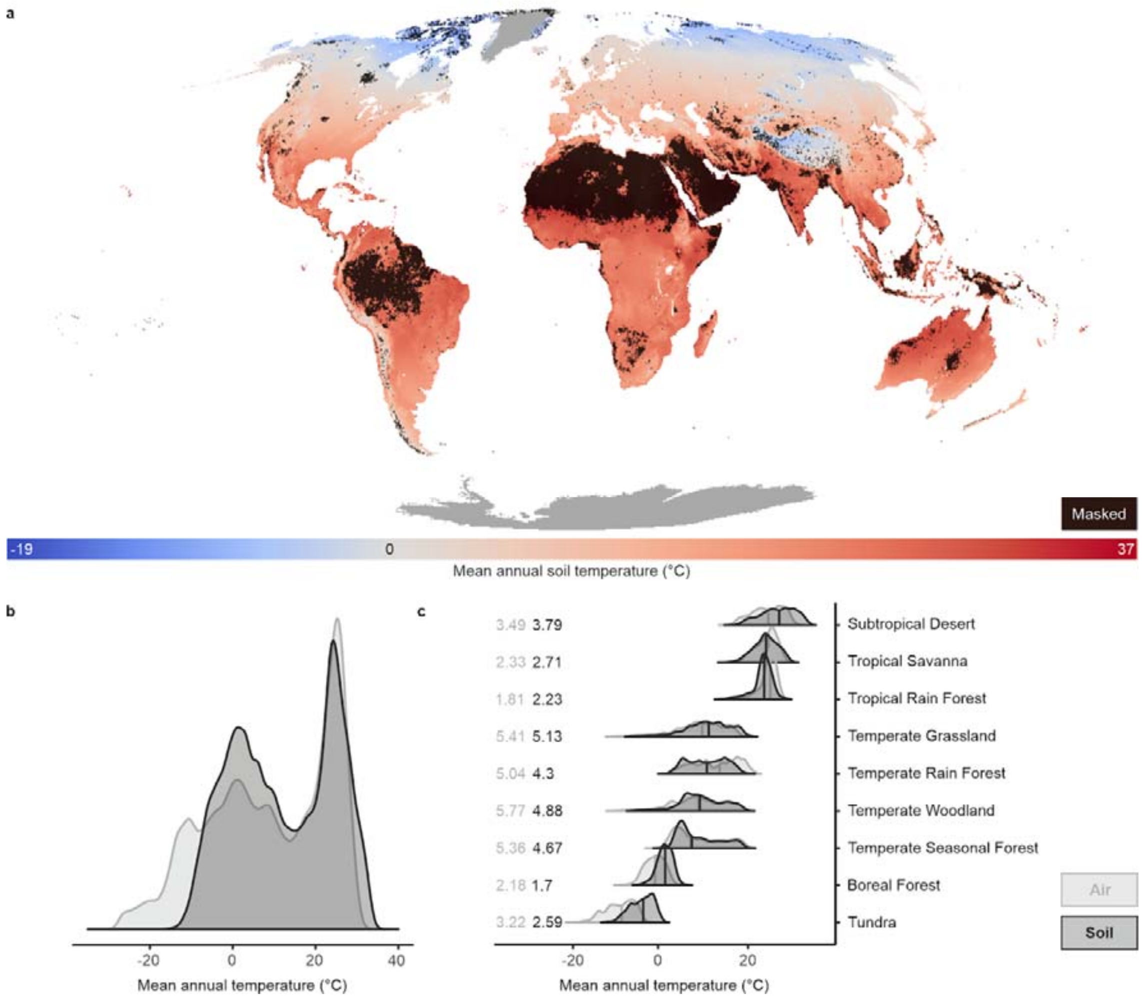

Figure 4: Mean annual soil temperature shows significantly lower spatial variability than air temperature. *(a) Global map of mean annual topsoil temperature (SBIO1, 0–5 cm depth, in °C), created by adding the monthly offset between soil and air temperature for the period 2000–2020 (Fig. 2) to the monthly air temperature from CHELSA for the period 1979–2013* [1] *and summarizing across all 12 months. A mask is used to exclude regions where our models are extrapolating (i.e., interpolation values in Fig. 3 are < 0.9, 18% of pixels). Dark grey represents regions outside the modelling area. (b–c) Density plots of mean annual soil temperature across the globe (b) and for each Whittaker biome separately (c) for SBIO1 (dark grey, soil temperature), compared with BIO1 from CHELSA (light grey, air temperature), created by extracting 1,000,000 random points from the 1-km^2 gridded bioclimatic products. The numbers in (c) represent the standard deviations of air temperatures (light grey) and soil temperatures (dark grey). Biomes are ordered according to the median annual soil temperature values from the highest temperatures (subtropical desert) to the lowest (tundra).*

Our results highlight clear biome-specific shifts in temperature between air and soil, as well as a significant reduction in the spatial variation in temperature, especially in cold and cool biomes. The observed impact of macroclimate on the temperature offset implies that soil temperatures will not warm at the same rate as air temperatures when climate warms. Indeed, one degree of air temperature warming can result in either a bigger or a smaller equivalent of soil temperature change, depending on where along the macroclimatic gradient it is occurring. This will impact cold biome soils most strongly, as they not only experience the largest temperature offsets and reductions in climate range compared to air temperature, but they are also expected to experience the strongest magnitude of climate warming (Fig. 4b, c)[54-57]. Similarly, changes in precipitation regimes and thus soil moisture can significantly alter the relationship between air and soil temperature, with critical implications for soil moisture-atmosphere feedbacks[9]. Importantly, future research should thus not only use soil temperature data as provided here to study belowground ecological processes[4,40,58], it should also urgently investigate future scenarios of soil climate warming in light of changing air temperature and precipitation, with the necessary spatial resolution to incorporate the uncovered non-linear relationships[59].

Conclusions

We observed large spatiotemporal heterogeneity in the global offset between soil and air temperature, often in the order of several degrees. Soil temperature is non-linearly related to air temperature at the global scale, implying that air temperature is not a suitable proxy for temperature conditions near or in the soil. However, we have provided the means to correct for these important regional mismatches. By making our global soil temperature maps and the underlying monthly offset data available openly, we offer gridded soil temperature data, based on *in situ* measurements for climate research, ecology, agronomy and other life and environmental sciences. These maps bring us one step closer to climate data exactly where it matters the most for most terrestrial organisms[6,7,48].

The biome-specific and seasonally variable offsets between air and soil temperature quantified here impact ecological relationships and bias predictions of current and future climate impacts[8,34-36,57,60]. Temperature in the topsoil rather than in the air ultimately defines the species' distributions and performance of most terrestrial speices, as well as many ecosystem functions at or below the soil surface[28-31]. As ecosystem functions are highly correlated with temperature, soil temperature rather than air temperature should be the preferred predictor for estimating their rates and temperature thresholds[61-63]. Correcting for the non-linear relationship between air and soil temperature is vital for all fields investigating abiotic and biotic processes related to terrestrial environments[64]. Indeed, soil temperature, macroclimate and land-use change will interact to define the future climate as experienced by organisms, and high-resolution soil temperature data is needed to tackle the on-going challenges as well as the ones ahead of us.

Methods

Data acquisition

Analyses are based on SoilTemp, a global database of microclimate time series[4]. We compiled soil temperature measurements from 9362 sensors from 60 countries, using both published and unpublished data sources (Fig. 1, Extended data Fig. 1). We used time series spanning a minimum of one month and a temporal resolution of four hours or less. Sensors of any type (Extended data Table 4) were included, if they measured *in situ*. Sensors in experiments manipulating the local climate such as open-top chambers, rain-out shelters or vegetation-removal experiments were excluded, except for control plots. Most data (> 90%) comes from low-cost rugged microclimate sensors such as iButtons (Maxim Integrated, USA), with measurement errors of around 0.5–1°C, while in a minority of cases sensors with higher meteorological specifications were used, such as industrial or scientific grade thermocouples and thermistors. Data included both soil temperature sensors at long-term weather stations as well as short-term regional networks of microclimate measurements. By combining these two types of data, a much higher spatial density of sensors and broader distribution of microhabitats could be obtained than when using weather station data only.

About 68% of data fell between 2010 and 2020 and 93% between 2000 and 2020; we thus focus on the latter period in our further analyses. Additionally, given the relatively short time frame covered by most individual sensors (mean duration 2.9 years, median duration 1.0 year, ranging from 1 month to 41 years) – we were not able to test for systematic differences in temperature offset between old and recent data sets, and thus do not correct for this in our models. We strongly urge future studies to assess such temporal dynamics in the offset. Currently long-term data at hand are too scarce to address this potential issue.

For each of the 9362 time series, we calculated monthly mean, minimum (5% percentile of all monthly values) and maximum (95% percentile) temperature, after checking all our time series data for plausibility and erroneous data. Months with more than one day of missing data, either at the beginning or end of the measurement period, or due to logger malfunctioning during measurement, were excluded, resulting in a final subset of 380,676 months of soil temperature time series that were used for further analyses. For each sensor with more than twelve months of data, we calculated moving averages of annual mean temperature, using each consecutive month as a starting month and calculating the mean temperature including the next eleven months. We used these moving averages to make maximal use of the full temporal extent covered by each sensor, because each time series spanned a different time period, often including parts of calendar years only. Next, these moving averages were further summarized to one mean annual average per 1 km^2 pixel (see below, under '*Global and biome-level analyses*').

The database contained sensors measuring temperature at depths between 0 and 200 cm below the ground surface. Sensors recording several measurements at the same site but located at different (vertical) depths were included separately. Sensors were grouped in different soil depth categories (0–5, 5–15, 15–30, 30–60, 60–100, 100–200 cm, Extended data Table 5) to incorporate the effects of soil temperature dampening. We limited our analyses to the topsoil (0–5 cm) and the second soil layer (5–15 cm), as we currently lack sufficient global coverage to make trustworthy models in deeper soil layers (8,519 (91%) sensors in the two upper layers).

We tested for potential bias in temporal resolution (i.e., measurement interval) by calculating mean, minimum and maximum temperature for a selection of 2,000 months for data measured every 15 minutes, and the same data aggregated to 30, 60, 90, 120 and 240 minutes. Monthly mean, minimum and maximum temperatures calculated with any of the aggregated datasets differed on average less than 0.2°C from the one with the highest temporal resolution. We were thus confident that pooling data with different temporal resolutions would not significantly affect our results.

Temperature offset calculation

For each monthly value at each sensor location (see Extended data Table 6 for number of data points per month), we extracted the corresponding monthly means of the 2 m air temperature from the European Centre for Medium-Range Weather (ECMWF) Forecast's 5^{th} reanalysis (ERA5) (from 1979 thus 1981) and ERA5-Land from 1981 till 2020[65]. The latter dataset models the global climate with a spatial resolution of 0.08 × 0.08 degrees (approximately 9 × 9 km) with an hourly resolution, converted into monthly means using daily means for the whole month. Similarly, monthly minima and maxima were obtained from TerraClimate[66] for the period 2000 thus 2020 at a 0.04 × 0.04 degrees (≈ 4 × 4 km) resolution. Monthly means for TerraClimate were not available, we therefore estimated them by averaging the monthly minima and maxima. Finally, we also obtained monthly mean temperatures from CHELSA[1] for the period 2000 thus 2013 at a 30 × 30 arc second (≈ 1 × 1 km) resolution. In our modelling exercises (see chapter 'Integrative modelling' below), we opted for using the mean temperature offsets as calculated based on ERA5 rather than on CHELSA, as the latter dataset only included monthly data up till 2013. While CHELSA's higher spatial resolution is definitely an advantage, it insufficiently overlapped with the time period covered by our *in situ* measurements (2000 thus 2020). The temperature offsets based on the CHELSA-dataset were thus only used for comparative purposes. We used TerraClimate to model offsets in monthly minimum and maximum temperature.

The offset between the *in situ* measured soil temperature in the SoilTemp database and the 2 m free-air temperature obtained from the air-temperature grids (ERA5, TerraClim and CHELSA) were calculated by subtracting the monthly mean air temperature from the monthly mean soil temperature. Positive offset values indicate a measured soil temperature higher than gridded air temperature, while negative offset values represent cooler soils. Similarly, monthly minimum and maximum air temperatures were subtracted from minimum and maximum soil temperatures, respectively. Monthly minima and maxima of the soil temperature were calculated as respectively the 5% lowest and highest instantaneous measurement in that month, to correct for outliers, which can be especially pronounced at the soil surface[67]. As a result, patterns in minima and maxima are more conservative estimates than if we had used the absolute lowest and highest value.

We calculated moving annual averages of the gridded air temperature data similar to those we computed for the soil temperature. These were used to create annual temperature offset values following the same approach as above.

Importantly, the temperature offset used here is a result of three key groups of drivers: (1) height effects (2 m versus 0–15 cm below the soil surface); (2) environmental or habitat effects (e.g., spatial variability in vegetation, snow or topography); and (3) scale effects (resolution of gridded air temperature)[4]. We investigate the potential role of scale effects by comparing free-air temperature data sources with different resolutions (ERA5, TerraClimate and CHELSA, see below). Height effects and environmental effects are however not disentangled here, as the offset we propose aims to incorporate both the difference between air and soil temperature (vertically), as well we the difference between free-air macroclimate and *in situ* microclimate (horizontally) in one measure[4]. While it can be argued that it would be better to treat both separately, this would require a similar database of coupled *in situ* air and soil temperature measurements, which is not yet available. Using *in situ* measured air temperature would also potentially solve spatial mismatches (i.e. spatially averaged air temperature represents the whole 1 to 9 km pixel, depending on pixel size, not only the exact location of the sensor). However, coupled air and soil temperature measurements are not only rare, but the air temperature measurements also have large measurement errors of up to several degrees when using non-standardized sensors, loggers and shielding[68]. Using *in situ* measured air temperature without correction for these measurement errors would thus be misleading.

Global and biome-level analyses

For the purpose of visualization, annual temperature offsets were first averaged in hexagons with a resolution of approximately 70,000 km², using the dggridR-package in R[69] (Fig. 1). Next, we plotted mean, minimum and maximum annual soil temperature as a function of corresponding free-air temperature from ERA5, TerraClimate and CHELSA and used generalized additive models (GAMs, package mgcv; [70]) to visualise deviations from the 1:1-line (i.e. temperature offsets deviating from zero, Extended data Figs. 3–5).

All annual and monthly values within each soil depth category and falling within the same 1-km² pixel were aggregated as a mean, resulting in a total of ~1,200 unique pixels at 0–5 cm, and ~1,000 unique pixels at 5–15 cm, across the globe (Extended data Table 6). This averaging includes summarizing the data over space, i.e., multiple sensors within the same 1-km² pixel, and time, i.e., data from multi-year time series from a certain sensor, to reduce spatial and temporal autocorrelation and high imbalance in sampling intensity. We assigned these 1-km² averages to the corresponding Whittaker biome of their georeferenced location, using the package *plotbiomes* in R (Fig. 1 c, d, Extended data Table 1[71]). We ranked biomes based on their offset and compared this with the mean annual precipitation in each biome (Fig. 1b). This was done separately for each air temperature data source (ERA5, TerraClimate and CHELSA), soil depth (0–5 cm, 5–15 cm) and time frame (ERA5 1979–2020, 2000–2020), as well as for the offset between monthly minimum and maximum soil temperature and the minimum and maximum free-air temperature from TerraClimate (Extended data Fig. 2). Our analyses showed that patterns were robust to the spatial variation in spatial resolution, sensor depth, climate interpolation method and temporal scale (Extended data Figs. 2-5).

Acquisition of global variable layers

To create spatial predictive models of the offset between *in situ* soil temperature and large-scale free-air temperature, we first sampled a stack of global map layers at each of the sensor locations within the data set. These layers included macroclimatic, soil texture and physiochemical information, vegetation, radiation and topographic indices and anthropogenic variables. Details of all layers, including descriptions, units, and source information, are described in Supplementary Table 1. In short, information about soil texture, structure and physiochemical properties was obtained from SoilGrids (version 2[72]), limited to the upper soil layer (top 5 cm). Climate information (i.e., monthly mean, maximum and minimum temperature, monthly precipitation) was obtained from CHELSA (version 2017[1]), which includes climate data averaged across 1979–2013, and from WorldClim (version 2[73]). Monthly snow probability is based on a pixel-wise frequency of snow occurrence (snow cover > 10%) in MODIS daily snow cover products (MOD10A1 & MYD10A1[74]) in 2001–2019. Spectral vegetation indices (i.e., averaged MODIS NDVI product MYD13Q1) and surface reflectance data (i.e., MODIS MCD43A4) were obtained from the Google Earth Engine Data Catalog (developers.google.com/earth-engine/datasets) and averaged from 2015 to 2019. Landcover and topographic information were obtained from EarthEnv[75]. Aridity index and potential evapotranspiration (PET) layers were obtained from CGIAR[76]. Anthropogenic information (population density) was obtained from the EU JRC (ghsl.jrc.ec.europa.eu/ghs_pop2019.php). Aboveground biomass data were obtained from GlobBiomass[77]. Resolved ecoregion classifications were used to categorize sampling locations into biomes[78]. With this set of variables, we included information on all different categories of drivers of soil temperature[4]. The final set of variables included a set of 24 ‘static’ variables and 7 monthly layers (i.e., macroclimate, cloud cover, solar radiation, water vapour pressure, and snow cover). Due to masked pixels in Northern Hemisphere high-latitude regions in January and December in the cloud cover layers as a result of the lack of daylight, we excluded cloud cover as an explanatory variable for these months (i.e., 'EarthEnvCloudCover_MODCF_monthlymean_XX', with XX representing the months in two-digit form Supplementary Table 1).

All variable map layers were reprojected and resampled to a unified pixel grid in EPSG:4326 (WGS84) at 30 arc-sec resolution (approximately 1 km^2 at the equator). Areas covered by permanent snow or ice (e.g., the Greenland ice cap, glaciated mountain ranges, identified using SoilGrids) were excluded from the analyses. Antarctic sampling points were excluded from the modelling data set owing to the limited coverage of several covariate layers in the region.

Integrative modelling

To generate global maps of monthly temperature offsets (Fig. 3), we trained random forest (RF) models for each month, using the temperature offsets and the above-mentioned global variable layers. We used a geospatial modelling pipeline as developed by Van Den Hoogen, et al. [2].

We performed a grid search procedure to tune the RF models across a range of 122 hyperparameter settings (variables per split: 2–12, minimum leaf population: 2–12). During this procedure, we assessed each model's performance using k-fold cross-validation (using k = 10; folds assigned randomly, stratified per biome), for each of the 122 models. The models' mean and standard deviation values were the basis for choosing the best model of all evaluated models. This procedure was repeated for each month separately for two soil depth layers (0–5 cm, 5–15 cm), for offsets in mean, minimum and maximum temperature. The importance of explanatory variables was assessed using the variable importance and ordered by mean variable importance across all models. This variable importance adds up the decreases in the impurity criterion (i.e., the measure on which the local optimal condition is chosen) at each split of a node for each individual variable over all trees in the forest[2].

All geospatial modelling was performed on Google Earth Engine[79] using the Python API.

Model uncertainty

To assess the uncertainty in the monthly models after aggregating at the pixel level, we performed a stratified bootstrapping procedure, with total size of the bootstrap samples equal to original training data. Using biome as a stratification category, we ensured the samples included in each of the bootstrap training collections were proportionally representative for each biome's total area. Next, we trained RF models (with the same hyperparameters as selected during the grid-search procedure) using each of 100 bootstrap iterations. Each of these trained RF models was then used to classify the covariate layer stack, to generate per-pixel 95% confidence intervals and standard deviation for the modelled monthly offsets (Fig. 3a, Extended data Fig. 7a). The mean R^2 value of the RF models for the monthly mean temperature offset was 0.70 (from 0.64 to 0.78) at 0-5 cm and 0.76 (0.63–0.85) at 5 to 15 cm across all twelve monthly models. Mean RMSE of the models was 2.20°C (1.94–2.51°C) at 0–5 cm, and 2.06°C (1.67–2.35°C) at 5–15 cm.

Importantly, model uncertainty as reported in Fig. 3a and Extended data Fig. 7a comes on top of existing uncertainties in (1) *in situ* soil temperature measurements and (2) the ERA5 macroclimate models as used in our models. However, both of those are usually under 1°C[21,65].

To assess the spatial extent of extrapolation due to incomplete global coverage of the training data, we first performed a PCA (Principal Component Analysis) on the full environmental space covered by the monthly training data, including all explanatory variables as used in the models, and then transformed the composite image into the same PC spaces as of the sampled data[2]. Next, we created convex hulls for each of the bivariate combinations from the first 10 to 12 PCs (covering more than 90% of the sample space variation, with the number of PCs depending on the month). Using the coordinates of these convex hulls, we assessed whether each pixel fell within or outside each of these convex hulls, and calculated the percentage of bivariate combinations for which this was the case (Fig. 3b, Extended data Fig. 7b). This process was repeated for each month, and each of the two depth intervals individually. These maps are important as the used machine-learning techniques are not suitable for extrapolation beyond the range covered by the environmental variables included in the original calibration dataset, and are provided as potential spatial masks to remove or reduce the weighting of the pixels for which predictions are beyond the range of values covered by the models during calibration. To assess this further, we used a spatial leave-one-out cross-validation analysis to test for spatial autocorrelation in the data set (Extended data Fig. 14)[2]. This approach trains a model for each sample in the data set on all remaining samples, excluding data points that fall within an increasingly large buffer around that focal sample. Results show lowest confidence for May to September at 5–15 cm, likely driven by uneven global coverage of data points.

Soil bioclimatic variables

The resulting global maps of the annual and monthly offsets between mean, minimum and maximum soil and air temperature were used to calculate relevant bioclimatic variables (following the definition used in CHELSA, BIOCLIM, ANUCLIM and WorldClim [1,73,80,81], Fig. 4, Extended data Figs. 12, 13). We calculated 11 soil bioclimatic layers (SBIO): SBIO1 = annual mean temperature; SBIO2 = mean diurnal range (mean of monthly (max temp - min temp)); SBIO3 = isothermality (SBIO2/SBIO7) (×100); SBIO4 = temperature seasonality (standard deviation ×100); SBIO5 = max temperature of warmest month; SBIO6 = min temperature of coldest month; SBIO7 = temperature annual range (SBIO5-SBIO6); SBIO8 = mean temperature of wettest quarter; SBIO9 = mean temperature of driest quarter; SBIO10 = mean temperature of warmest quarter; and SBIO11 = mean temperature of coldest quarter. First, we calculated monthly soil mean, maximum and minimum temperatures by adding monthly temperature offsets to the respective CHELSA monthly mean, maximum and minimum temperatures[1]. Next, following arithmetic outlined in O'Donnell and Ignizio [82], we used these soil temperature layers to compute the SBIO layers. Wettest, and driest quarters were identified for each pixel based on CHELSA's monthly values.

Temporal mismatch

There is a temporal mismatch between the period covered by CHELSA (1979-2013) and by our *in situ* measurements (2000-2020) which prevented us from directly using CHELSA-climate to calculate the temperature offsets as used in our models. This temporal mismatch might affect the offsets as calculated here, because it is possible that the relationship of the temperature offset with macroclimate will change over time as the climate warms.

However, we are confident that our results are sufficiently robust to withstand this mismatch, given that we found high consistency in offset patterns between different time frames and air temperature data sets examined (Extended data Figs. 2–5). Nevertheless, we strongly urge future research to disentangle these potential temporal dynamics, especially given the increasing rate at which the climate is warming[55,83]. Similarly, a potential bias could come from the mismatch in method and resolution between ERA5 – as used to calculate the temperature offsets – and CHELSA, as used to create the bioclimatic variables. However, even though temperature offsets have slightly larger variation when based on the coarser-grained ERA5-data than on the finer-grained CHELSA-data, Extended data Figs. 5 and 2–4 show that relationships between soil and air temperature are largely consistent in all biomes and across the whole global temperature gradient. Importantly, the larger offsets thus created additional random scatter, yet it did not create consistent bias.

Data visualizations were effected using R version 4.0.2[84]. All maps were plotted using the Mollweide projection to avoid the large distortions at high latitudes that are present in many other common projections.

Data availability

Soil bioclimatic layers are available on Zenodo (link published on https://soiltemp.weebly.com). Soil bioclim layers SBIO1-11 are also directly available in Google Earth Engine under projects/crowtherlab/soil_bioclim/soil_bioclim_0_5cm and projects/crowtherlab/soil_bioclim/soil_bioclim_5_15cm.

Acknowledgements

JJL received funding from the Research Foundation Flanders (grant nr. 12P1819N) The project received funding from the Research Foundation Flanders (grants nrs, G018919N, W001919N). JA received funding from the University of Helsinki, Faculty of Science (MICROCLIM, grant nr. 7510145) and Academy of Finland Flagship (grant no. 337552). PDF, CM and PV received funding from the European Research Council (ERC) under the European Union's Horizon 2020 research and innovation programme (ERC Starting Grant FORMICA 757833). JK received funding from the Arctic Interactions at the University of Oulu and Academy of Finland (318930, Profi 4), Maa- ja vesitekniikan tuki ry., Tiina and Antti Herlin Foundation, Nordenskiöld Samfundet and Societas pro Fauna et Flora Fennica. MK received funding from the Czech Science Foundation (grant nr. 20-28119S) and the Czech Academy of Sciences (grant nr. RVO 67985939). TC received funding from DOB Ecology. National Geographic Society grant no. 9480-14 and WW-240R-17. MA recieved funding from CISSC (program ICRP (grant nr:2397) and INSF (grant nr: 96005914). The Royal Botanic Garden Edinburgh is supported by the Scottish Government's Rural and Environment Science and Analytical Services Division. JMA received funding from the Funding Org. Qatar Petroleum (grant nr. QUEX-CAS-QP-RD-18/19). JMA received funding from the European Union's Horizon 2020 research and innovation program (grant no. 678841) and from the Swiss National Science Foundation (grant no. 31003A_176044). JA was supported by research grants LTAUSA19137 (program INTER-EXCELLENCE, subprogram INTER-ACTION) provided by Czech Ministry of Education, Youth and Sports and the Czech Science Foundation (20-05840Y) and 20-05840Y of the Czech Science Foundation. AA was supported by the Ministry of

Science and Higher Education of the Russian Federation (grant FSRZ-2020-0014). SN, UAT, JJA, and JvO received funding from the Independent Research Fund Denmark (7027-00133B). LvdB, MYB and RC acknowledge funding from the German Research Foundation within the Priority Program SPP-1803 “EarthShape: Earth Surface Shaping by Biota” (grant BA 3843/6-1). PB was supported by grant project VEGA of the Ministry of Education of the Slovak Republic and the Slovak Academy of Sciences No. 2/0132/18. Forest Research received funding from the Forestry Commission (climate change research programme). JCB acknowldeges the support of Universidad Javeriana. JLBA received funding from the Dirección General de Cambio Climático del Gobierno de Aragón; JLBA acknowledges fieldwork assistance by Ana Acín, the Ordesa y Monte Perdido National Park, and the Servicio de Medio Ambiente de Soria de la Junta de Castilla y León. RGB and MPB received funding from BECC - Biodiversity and Ecosystem services in a Changing Climate. MPB received funding from The European Union’s Horizon 2020 research and innovation program under the Marie Skłodowska-Curie Grant Agreement No. 657627 and The Swedish Research Council FORMAS – future research leaders No. 2016-01187. JB received funding from the Czech Academy of Sciences (grant nr. RVO 67985939). NB received funding from the SNF (grant numbers 40FA40_154245, 20FI21_148992, 20FI20_173691, 407340_172433) and from the EU (contract no. 774124). ICOS EU research infrastructure. EU FP7 NitroEurope. EU FP7 ECLAIRE. The authors from Biological Dynamics of Forest Fragments Project, PDBFF, Instituto Nacional de Pesquisas da Amazônia, Brazil were supported by the MCTI/CNPq/FNDCT – Ação Transversal n°68/2013 – Programa de Grande Escala da Biosfera-Atmosfera na Amazônia – LBA; Project “Como as florestas da Amazônia Central respondem às variações climáticas? Efeitos sobre dinâmica florestal e sinergia com a fragmentação florestal.”. to The EUCFLUX Cooperative Research Program and Forest Science and Research Institute-IPEF. NC acknowledges funding by Stelvio National Park. JC was funded by the Spanish government grant CGL2016-78093-R. ANID-FONDECYT 1181745 AND INSTITUTO ANTARTICO CHILENO (INACH FR-0418). SC received funding from the German Research Foundation (grant no. DFG– FZT 118, 202548816). The National Science Foundation, Poland (grant no. UMO-2017/27/B/ST10/02228), within the framework of the “Carbon dioxide uptake potential of sphagnum peatlands in the context of atmospheric optical parameters and climate changes”(KUSCO2) project. SLC received funding from the South African National Research Foundation and the Australian Research Council. FM, MČ, KU and MU received funding from Slovak Research and Development Agency (no. APVV-19-0319). Instituto Antartico Chileno (INACH_RT-48_16), Iniciativa Científica Milenio Núcleo Milenio de Salmónidos Invasores INVASAL, Institute of Ecology and Biodiversity (IEB), CONICYT PIA APOYO CCTE AFB170008. PC is supported by NERC core funding to the BAS 'Biodiversity, Evolution and Adaptation Team. EJC received funding from the Norwegian Research Council (grant number 230970). GND was supported by NERC E3 doctoral training partnership grant (NE/L002558/1) at the University of Edinburgh and the Carnegie Trust for the Universities of Scotland. Monitoring stations on Livingston Island, Antarctica were funded by different research projects of the Gobern of Spain (PERMAPLANET CTM2009-10165-E; ANTARPERMA CTM2011-15565-E; PERMASNOW CTM2014-52021-R), and the PERMATHERMAL arrangement between the University of Alcalá and the Spanish Polar Committee. GN received funding from the Autonomous Province of Bolzano (ITA). The infrastructure, part of the UK Environmental Change Network, was funded historically in part by ScotNature.and and NERC National Capability LTS-S: UK-SCAPE; NE/R016429/1). JD was supported by the Czech Science Foundation (GA17-19376S) and MSMT (LTAUSA18007). ED received funding from the Kempe Foundation (JCK-1112 and JCK-1822). The infrastructure was supported by the Ministry of Education, Youth and Sports of the Czech Republic within the National Sustainability Programme I (NPU I), grant number LO1415 and by the project for national infrastructure support CzeCOS/ICOS Reg.No. LM2015061. NE received funding from the German Research Foundation (DFG– FZT 118, 202548816). BE received funding from the GLORIA-EU project no EVK2-CT2000-00056, the Autonomous Province of Bolzano (ITA), from the Tiroler Wissenschaftsfonds and from the University of Innsbruck. RME was supported by funding to the SAFE Project from the Sime Darby Foundation. OF received funding from the German Research Foundation (DFG– FZT 118, 202548816). MF was funded by the German Federal Ministry of Education and Research (BMBF) in the context of The Future Okavango (Grant No. 01LL0912) and SASSCAL (01LG1201M; 01LG1201N) projects. RAG received funding from Fondecyt 11170516 and CONICYT PIA AFB170008. MBG received funding from National Parks (DYNBIO, #1656/2015) and The Spanish Research Agency (VULBIMON, #CGL2017-90040-R). MG received funding from the Swiss National Science Foundation (ICOS-CH Phase 2 20FI20_173691). FG received funding from the German Research Foundation (DFG– FZT 118, 202548816). KG received funding from the UK Biotechnology and Biological Research Council (grant = 206/D16053). SG was supported by the Research Foundation Flanders (FWO) (project G0H1517N). SH and ARB received funding through iDiv funded by the German Research Foundation (DFG– FZT 118, 202548816). LH received funding from the Czech Science Foundation (grant nr. 20-28119S) and the Czech Academy of Sciences (grant nr. RVO 67985939). MH received funding from the Baden-Württemberg Ministry of Science, Research and Arts via the project DRIeR (Drought impacts, processes and resilience: making the in-visible visible). LH received funding from International Polar Year, Weston Foundation, and ArcticNet. DH received funding from Natural Sciences and Engineering Council (Canada) (RGPIN-06691). TTH received funding from Independent Research Fund Denmark (grant no. 8021-00423B) and Villum Foundation (grant no. 17523). Ministry of Education, Youth and Sports of the Czech Republic (projects LM2015078, VAN2020/01 and CZ.02.1.01/0.0/0.0/16_013/0001708). KH and CG received funding from Bolin Centre for Climate Research, Stockholm University and from the Swedish research council Formas [grant n:o 2014-00530 to KH]. JJ received funding from the Funding Org. Swedish Forest Society Foundation (grant nr. 2018-485-Steg 2 2017) and Swedish Research Council FORMAS (grant nr. 2018-00792). Project LAS III 77/2017/B entitled: \"Estimation of net carbon dioxide fluxes exchanged between the forest ecosystem on post-agricultural land and between the tornado-damaged forest area and the atmosphere using spectroscopic and numerical methods\", source of funding: General Directorate of State Forests, Warsaw, Poland. AJ received funding from the German Federal Ministry of Education and Research BMBF (Grant Nr. FKZ 031B0516C SUSALPS) and the Oberfrankenstiftung (Grant Nr. OFS FP00237). ISJ received funding from the Energy Research Fund (NÝR-11 - 2019, NÝR-18 - 2020). TJ was supported by a UK NERC Independent Research Fellowship (grant number: NE/S01537X/1). RJ received funding from National Science Centre of Poland (grant number: 2016/21/B/ST10/02271) and Polish National Centre for Research and Development (grant number: Pol-Nor/203258/31/2013). VK received funding from the Czech Academy of Sciences (grant nr. RVO 67985939). AAK received funding from SAC-ISRO, India (HIMADRI Project). NK received funding from FORMAS, VR, support from the research infrastructure ICOS. KJ received funding from the EU Horizon2020 INFRAIA project eLTER-PLUS (871128), the project LTER-CWN (FFG, F&E Infrastrukturförderung, project number 858024) and the Austrian Climate Research Program (ACRP7 – CentForCSink – KR14AC7K11960). BK received funding from the National Research, Development and Innovation Fund of Hungary (grant nr. K128441). Ministry of Education, Youth and Sports of the Czech Republic (projects LM2015078 and CZ.02.1.01/0.0/0.0/16_013/0001708). Project B1-RNM-163-UGR-18-Programa Operativo FEDER 2018, partially funded data collection. Norwegian Research Council (NORKLIMA grants #184912 and #244525) awarded to Vigdis Vandvik. MM received funding from the Czech

Science Foundation (grant nr. 20-28119S) and the Czech Academy of Sciences (grant nr. RVO 67985939). Project CONICYT-PAI 79170119 awarded to Roy Mackenzie. This work was partly funded by project MIUR PON Cluster OT4CLIMA. RM received funding from the SNF project number 407340_172433. FM received funding from the Stelvio National Park. PM received funding from AIAS-COFUND fellowship programme supported by the Marie Skłodowska- Curie actions under the European Union's Seventh Framework Pro-gramme for Research, Technological development and Demonstration (grant agreement no 609033) and the Aarhus University Research Foundation, Denmark. RM received funding from the Ministry of Education, Youth and Sports of the Czech Republic (project LTT17033). SM and VM received funding from EU FP6 NitroEurope (grant nr. 17841), EU FP7 ÉCLAIRE (grant nr. 282910), the Ministry of Education and Science of Ukraine (projects nr. 505, 550, 574, 602), GEF-UNEP funded "Toward INMS" project (grant nr. NEC05348) and ENI CBC BSB PONTOS (grant nr. BSB 889). STM received funding from New Frontiers in Research Fund-Exploration (grant nr. NFRF-2018-02043) and NSERC Discovery. MMR received funding from the Australian Research Council Discovery Early Career Research Award (grant nr. DE180100570). JAM received funding from the National Science Foundation (DEB 1557094), International Center for Advanced Renewable Energy and Sustainability (I-CARES) at Washington University in St. Louis, ForestGEO, and Tyson Research Center. IM-S was funded by the UK Natural Environment Research Council through the ShrubTundra Project (NE/M016323/1). MBN received funding from FORMAS, VR, Kempe Foundations support from the research infrastructures ICOS and SITES. MDN received funding from CONICET (grant nr. PIP 112-201501-00609). Spanish Minsitry of Science grant PID2019-110521GB-I00 and Catalan government grant 2017-1005. French National Research Agency (ANR) in the frame of the Cluster of Excellence COTE (project HydroBeech, ANR-10-LABX-45). VLIR-OUS, under the Institutional University Coorperation programme (IUC) with Mountains of the Moon University. Max Planck Society (Germany), RFBR, Krasnoyarsk Territory and Krasnoyarsk Regional Fund of Science, project number 20-45-242908. Estonian Research Council (PRG609), and the European Regional Development Fund (Centre of Excellence EcolChange). Canada-Denmark Arctic Research Station Early Career Scientist Exchange Program, from Polar knowledge Canada (POLAR) and the Danish Agency for Science and Higher Education. Fondecyt 1180205 and CONICYT PIA AFB170008. MP received funding from the Funding Org. Knut and Alice Wallenberg Foundation (grant nr. 2015.0047), and acknowledges funding from the Swedish Research Council (VR) with contributing research institutes to both the SITES and ICOS Sweden infrastructures. MPB received funding from the Svalbard Environmental Protection Fund (grant project number 15/128) and the Research Council of Norway (Arctic Field Grant, project number 269957). RP received funding from the Ministry of Education, Youth and Sports of the Czech Republic (grant INTER-TRANSFER nr. LTT20017). LTSER Zone Atelier Alpes; Fédération FREE-Alpes. RP received funding from a Humboldt Fellowship for Experienced Researchers. RPu received founding from the Polish National Science Centre (grant project number 2017/27/B/NZ8/00316). ODYSSEE project (ANR-13-ISV7-0004, PN-II-ID-JRP-RO-FR-2012). Project SUBANTECO IPEV 136 (French Polar Institute Paul-Emile Victor), Zone Atelier CNRS Antarctique et Terres Australes, SAD Région Bretagne (Project INFLICT), BiodivERsa 2019-2020 BioDivClim call 'ASICS' (ANR-20-EBI5-0004). NSF grant #1556772 to the University of Notre Dame. Pavia University (Italy). OR received funding from EU-LEAP-Agri (RAMSES II), EU-DESIRA (CASSECS), EU-H2020 (SustainSahel), AGROPOLIS and TOTAL Foundations (DSCATT), CGIAR (GLDC). AR was supported by the Russian Science Foundation (Grant 18-74-10048). Parc national des Ecrins. JS received funding from Vetenskapsrådet grant nr (No: 2014-04270), ALTER-net multi site grant, River LIFE project (LIFE08 NAT/S/000266), Flexpeil. Helmholtz Association long-term research program TERENO (Terrestrial Environmental Observatories). PS received funding from the Polish Ministry of Science and Higher Education (grant nr. N N305 304840). AS recieved funding from the ETH Research grant (grant number ETH-27 19-1). LSC recevied funding from NSERC Canada Graduate Scholarship (Doctoral) Program; LSC was also supported by ArcticNet-NCE (insert grant #). Conselho Nacional de Desenvolvimento Científico e Tecnológico (141513/2017-9); Fundação Carlos Chagas Filho de Amparo à Pesquisa do Estado do Rio de Janeiro (E26/200.84/2019). ZS received funding from the SRDA (nr. APVV-16-0325) and from the ERDF (grant nr. ITMS 313011S735, CE LignoSilva). JS, MB, and CA received funding from core budget of ETH Zurich. State excellence Program M-V \"WETSCAPES\". AfricanBioServices project funded by the EU Horizon 2020 grant number 641918. The authors from KIT/IMK-IFU acknowldege the funding received within the German Terrestrial Environmental Observatories (TERENO) research program of the Helmholtz Association and from the Bavarian Ministry of the Environment and Public Health (UGV06080204000). Deutsche Forschungsgemeinschaft (DFG, German Research Foundation), project number 192626868, in the framework of the collaborative German-Indonesian research project CRC 990 (SFB): "EFForTS, Ecological and Socioeconomic Functions of Tropical Lowland Rainforest Transformation Systems (Sumatra, Indonesia)". MS received funding from the Ministry of Education, Youth and Sports of the Czech Republic (grant nr. INTER-TRANSFER LTT19018). TT received funding from the Swedish National Space Board (SNSB Dnr 95/16) and the CASSECS project supported by the European Union. HJDT received funding from the UK Natural Environment Research Council (NERC doctoral training partnership grant NE/L002558/1). German Science Foundation (DFG) GraKo 2010 \"Response\". PDT received funding from the MEMOIRE project (PN-III-P1-1.1-PD2016-0925). Arctic Challenge for Sustainability II (ArCS II; JPMXD1420318865). JU received funding from Czech Science Foundation (grant nr. 21-11487S). TU received funding from the Romanian Ministry of Education and Research (CCCDI - UEFISCDI -project PN-III-P2-2.1-PED-2019-4924 and PN2019-2022/19270201-Ctr. 25N BIODIVERS 3-BIOSERV)\r\n. AV received funding from RFBR project number 19-04-01234-a. GFV received funding from the Dutch Research Council NWO (Veni grant, no. 863.14.013). Australian Research Council Discovery Early Career Research Award DE140101611. FGAV received funding from the Portuguese Science Foundation (FCT) under CEECIND/02509/2018, CESAM (UIDP/50017/2020+UIDB/50017/2020), FCT/MCTES through national funds, and the co-funding by the FEDER, within the PT2020 Partnership Agreement and Compete 2020. Ordesa y Monte Perdido National Park. MVI received funding from the Spanish Ministry of Science and Innovation through a doctoral grant (FPU17/05869). JW received funding from the Czech Science Foundation (grant nr. 20-28119S) and the Czech Academy of Sciences (grant nr. RVO 67985939). CR and SW received funding from the Swiss Federal Office for the Environment (FOEN) and the de Giacomi foundation. YY received funding from the National Natural Science Foundation of China (Grant no. 41861134039 and 41941015). ZY received funding from the National Natural Science Foundation of China (grant nr. 41877458). FZ received funding from the Swiss National Science Foundation (grant nr. 172198 and 193645). PZ received funding from the Funding Org. Knut and Alice Wallenberg Foundation (grant no. 2015.0047). JL received funding from: (i) the Agence Nationale de la Recherche (ANR), under the framework of the young investigators (JCJC) funding instrument (ANR JCJC Grant project N°ANR-19-CE32-0005-01: IMPRINT); (ii) the Centre National de la Recherche Scientifique (CNRS) (Défi INFINITI 2018: MORFO); and the Structure Fédérative de Recherche (SFR) Condorcet (FR CNRS 3417: CREUSE).

Fieldwork in the Arctic got facilitated by funding from the EU INTERACT program. SN, UAT, JJA, and JvO would like to thank the field team of the Vegetation Dynamics group for their efforts and hard work. We acknowledge Dominique Tristan for letting access to the field. for the logistic support the crew of INACH and Gabriel de Castilla Station team on Deception Island. We thank the Inuvialuit and Kluane First Nations for the opportunity to work on their land. MAdP acknowledges fieldwork assistance and logistics support to Unidad de Tecnología Marina CSIC, and the crew of Juan Carlos I and Gabriel de Castilla Spanish Antarctic Stations, as well as to the different colleagues from UAH that helped on the instruments maintainance. ERF acknowledges fieldwork assistance by Martin Heggli. MBG acknowledges fieldwork and technical assistance by P Abadía, C Benedé, P Bravo, J Gómez, M Grasa, R Jimenez, H Miranda, B Ponz, J Revilla and P Tejero, and the Ordesa and Monte Perdido National Park staff. LH acknowledges field assistance by John Jacobs, Andrew Trant, Robert Way, Darroch Whitaker; I acknowledge the IInuit of Nunatsiavut, and the Cooperative Management Board of Torngat Mountains National Park for their support of this project and acknowledge that the field research was conducted on their traditional lands. We thank our many bear guides, especially Boonie, Eli, Herman, John, and Maria Merkuratsuk. AAK acknowledges field support of Akhtar Malik, Rameez Ahmad. Part of microclimatic records from Saxony was funded by the Saxon Switzerland National Park Administration. Tyson Research Center. JP acknowledges field support of Emmanuel Malet (Edytem) and Rangers of Reserves Naturelles de Haute-Savoie (ASTERS). practical help: Roel H. Janssen, N. Huig, E. Bakker, Schools in the tepåseförsöket, Forskar fredag, Erik Herberg. The support by the Bavarian Forest National Park administration is highly appreciated. Liesbeth acknowledges CONAF and onsite support from the park rangers from PN Pan de Azucar, PN La Campana, PN Nahuelbuta and from communidad agricola Quebrada de Talca. JL and FS acknowledge Manuel Nicolas and all forest officers from the Office National des Forêts (ONF) who are in charge of the RENECOFOR network and who provided help and local support for the installation and maintenance of temperature loggers in the field.

Author contributions

JJL and JL conceptualized the project, JJL, JvdH, MBA, PDF, MK, ML, IMDM, TWC, IN and JL designed the paper, the SoilTemp consortium acquired the data, JJL, JVDH, JK and PN analysed the data, JJL, JvdH, JA, MBA, PDF, JK, MK, ML, IMDM, TWC, JJB, SH, DHK, PN, BRS and KVM interpreted the analyses. All authors significantly revised the manuscript and approved it for submission.

The authors declare no competing interests.

Supplementary Information is available for this paper.

Correspondence and requests for materials should be addressed to Jonas Lembrechts (Jonas.lembrechts@uantwerpen.be).

References

1. Karger, D. N. *et al.* (2017). Climatologies at high resolution for the earth's land surface areas. *Scientific Data* 4, 170122.

2. Van Den Hoogen, J. *et al.* (2019). Soil nematode abundance and functional group composition at a global scale. *Nature* 572, 194-198.

3. Steidinger, B. S. *et al.* (2019). Climatic controls of decomposition drive the global biogeography of forest-tree symbioses. *Nature* 569, 404-408.

4. Lembrechts, J. *et al.* (2020). SoilTemp: call for data for a global database of near-surface temperature. *Global Change Biology* 26, 6616-6629.

5. Bramer, I. *et al.* (2018). Advances in monitoring and modelling climate at ecologically relevant scales. *Advances in Ecological Research* 58, 101-161.

6. Ashcroft, M. B. *et al.* (2014). Testing the ability of topoclimatic grids of extreme temperatures to explain the distribution of the endangered brush-tailed rock-wallaby (*Petrogale penicillata*). *Journal of Biogeography* 41, 1402-1413.

7. Lembrechts, J. J. *et al.* (2019). Comparing temperature data sources for use in species distribution models: From in-situ logging to remote sensing. *Global Ecology and Biogeography* 28, 1578-1596.

8. Zellweger, F. *et al.* (2020). Forest microclimate dynamics drive plant responses to warming. *Science* 368, 772-775.

9. Zhou, S. *et al.* (2021). Soil moisture–atmosphere feedbacks mitigate declining water availability in drylands. *Nature Climate Change*, 1-7.

10. Bruelheide, H. *et al.* (2018). Global trait–environment relationships of plant communities. *Nature Ecology & Evolution* 2, 1906.

11. Kissling, W. D. *et al.* (2018). Towards global data products of Essential Biodiversity Variables on species traits. *Nature Ecology & Evolution* 2, 1531-1540.

12. Kattge, J. *et al.* (2019). TRY plant trait database-enhanced coverage and open access. *Global Change Biology* 26, 119-188.

13. Lenoir, J. *et al.* (2020). Species better track climate warming in the oceans than on land. *Nature Ecology & Evolution* 4, 1044-1059.

14. Antão, L. H. *et al.* (2020). Temperature-related biodiversity change across temperate marine and terrestrial systems. *Nature Ecology & Evolution* 4, 927-933.

15. Senior, R. A. *et al.* (2019). Global loss of climate connectivity in tropical forests. *Nature Climate Change* 9, 623-626.

16. Soudzilovskaia, N. A. *et al.* (2015). Global patterns of plant root colonization intensity by mycorrhizal fungi explained by climate and soil chemistry. *Global Ecology and Biogeography* 24, 371-382.

17. Du, E. *et al.* (2020). Global patterns of terrestrial nitrogen and phosphorus limitation. *Nature Geoscience* 13, 221-226.

18. World Meteorological Organization. *Guide to Meteorological Instruments and Methods of Observation*. (WMO-No. 8., 2008).

19. Daly, C. (2006). Guidelines for assessing the suitability of spatial climate data sets. *International Journal of Climatology* 26, 707-721.

20. Körner, C. & Hiltbrunner, E. (2018). The 90 ways to describe plant temperature. *Perspectives in Plant Ecology, Evolution and Systematics* 30, 16-21.

21. Wild, J. *et al.* (2019). Climate at ecologically relevant scales: A new temperature and soil moisture logger for long-term microclimate measurement. *Agricultural and Forest Meteorology* 268, 40-47.

22. Zhang, Y. *et al.* (2018). Impacts of snow on soil temperature observed across the circumpolar north. *Environmental Research Letters* 13, 044012.

23. Zhang, Y. *et al.* (2008). Impact of snow cover on soil temperature and its simulation in a boreal aspen forest. *Cold Regions Science and Technology* 52, 355-370.
24. De Frenne, P. *et al.* (2019). Global buffering of temperatures under forest canopies. *Nature Ecology & Evolution* 3, 744-749.
25. Way, R. G. & Lewkowicz, A. G. (2018). Environmental controls on ground temperature and permafrost in Labrador, northeast Canada. *Permafrost and Periglacial Processes* 29, 73-85.
26. Geiger, R. *The climate near the ground*. (Harvard University Press, 1950).
27. Obu, J. *et al.* (2019). Northern Hemisphere permafrost map based on TTOP modelling for 2000–2016 at 1 km2 scale. *Earth-Science Reviews* 193, 299-316.
28. Portillo-Estrada, M. *et al.* (2016). Climatic controls on leaf litter decomposition across European forests and grasslands revealed by reciprocal litter transplantation experiments. *Biogeosciences* 13, 1621-1633.
29. Pleim, J. E. & Gilliam, R. (2009). An indirect data assimilation scheme for deep soil temperature in the Pleim–Xiu land surface model. *Journal of Applied Meteorology and Climatology* 48, 1362-1376.
30. Hursh, A. *et al.* (2017). The sensitivity of soil respiration to soil temperature, moisture, and carbon supply at the global scale. *Global Change Biology* 23, 2090-2103.
31. Gottschall, F. *et al.* (2019). Tree species identity determines wood decomposition via microclimatic effects. *Ecology and Evolution* 9, 12113-12127.
32. Davis, E. *et al.* (2020). Plant–Environment Interactions in the Low Arctic Torngat Mountains of Labrador. *Ecosystems*, 1-21.
33. Schimel, J. P. *et al.* (2004). Increased snow depth affects microbial activity and nitrogen mineralization in two Arctic tundra communities. *Soil Biology and Biochemistry* 36, 217-227.
34. Kearney, M. *et al.* (2009). The potential for behavioral thermoregulation to buffer "cold-blooded" animals against climate warming. *Proceedings of the National Academy of Sciences* 106, 3835-3840.
35. Opedal, O. H. *et al.* (2015). Linking small-scale topography with microclimate, plant species diversity and intra-specific trait variation in an alpine landscape. *Plant Ecology & Diversity* 8, 305-315.
36. Körner, C. & Paulsen, J. (2004). A world-wide study of high altitude treeline temperatures. *Journal of Biogeography* 31, 713-732.
37. Scherrer, D. *et al.* (2011). Elevational species shifts in a warmer climate are overestimated when based on weather station data. *International journal of Biometeorology* 55, 645-654.
38. Crowther, T. W. *et al.* (2016). Quantifying global soil carbon losses in response to warming. *Nature* 540, 104-108.
39. De Frenne, P. *et al.* (2021). Forest microclimates and climate change: importance, drivers and future research agenda. *Global change biology* In press.
40. De Frenne, P. *et al.* (2013). Microclimate moderates plant responses to macroclimate warming. *Proceedings of the National Academy of Sciences* 110, 18561-18565.
41. Hennon, P. E. *et al.* (2010). Influence of forest canopy and snow on microclimate in a declining yellow-cedar forest of Southeast Alaska. *Northwest Science* 84, 73-87.
42. Grünberg, I. *et al.* (2020). Linking tundra vegetation, snow, soil temperature, and permafrost. *Biogeosciences* 17, 4261-4279.
43. Wang, K. & Dickinson, R. E. (2012). A review of global terrestrial evapotranspiration: Observation, modeling, climatology, and climatic variability. *Reviews of Geophysics* 50.
44. Grundstein, A. *et al.* (2005). Snowpack control over the thermal offset of air and soil temperatures in eastern North Dakota. *Geophysical research letters* 32.
45. Greiser, C. *et al.* (2018). Monthly microclimate models in a managed boreal forest landscape. *Agricultural and Forest Meteorology* 250, 147-158.
46. Niittynen, P. *et al.* (2020). Fine-scale tundra vegetation patterns are strongly related to winter thermal conditions. *Nature Climate Change* 10, 1143-1148.

47. Myers-Smith, I. H. *et al.* (2020). Complexity revealed in the greening of the Arctic. *Nature Climate Change* 10, 106-117.
48. Niittynen, P. & Luoto, M. (2018). The importance of snow in species distribution models of arctic vegetation. *Ecography* 41, 1024-1037.
49. Gisnås, K. *et al.* (2016). Small-scale variation of snow in a regional permafrost model. *The Cryosphere* 10, 1201-1215.
50. Kearney, M. R. *et al.* (2019). A method for computing hourly, historical, terrain-corrected microclimate anywhere on Earth. *Methods in Ecology and Evolution* 11, 38-43.
51. Maclean, I. M. (2019). Predicting future climate at high spatial and temporal resolution. *Global Change Biology* 26, 1003-1011.
52. Ashcroft, M. B. & Gollan, J. R. (2012). Fine-resolution (25 m) topoclimatic grids of near-surface (5 cm) extreme temperatures and humidities across various habitats in a large (200 x 300 km) and diverse region. *International Journal of Climatology* 32, 2134-2148.
53. Whiteman, C. D. (1982). Breakup of temperature inversions in deep mountain valleys: Part I. Observations. *Journal of Applied Meteorology* 21, 270-289.
54. Overland, J. E. *et al.* (2014). Future Arctic climate changes: Adaptation and mitigation time scales. *Earth's Future* 2, 68-74.
55. GISTEMP Team (2021). GISS Surface Temperature Analysis (GISTEMP), version 4. *NASA Goddard Institute for Space Studies*.
56. Chen, L. *et al.* (2021). Significant shallow–depth soil warming over Russia during the past 40 years. *Global and Planetary Change* 197, 103394.
57. Cooper, E. J. (2014). Warmer shorter winters disrupt Arctic terrestrial ecosystems. *Annual Review of Ecology, Evolution, and Systematics* 45, 271-295.
58. Lembrechts, J. *et al.* (2018). Incorporating microclimate into species distribution models. *Ecography* 42, 1267-1279.
59. Lembrechts, J. J. & Nijs, I. (2020). Microclimate shifts in a dynamic world. *Science* 368, 711-712.
60. Graae, B. J. *et al.* (2018). Stay or go–how topographic complexity influences alpine plant population and community responses to climate change. *Perspectives in Plant Ecology, Evolution and Systematics* 30, 41-50.
61. Schimel, D. S. *et al.* (1996). Climate and nitrogen controls on the geography and timescales of terrestrial biogeochemical cycling. *Global Biogeochemical Cycles* 10, 677-692.
62. Coûteaux, M.-M. *et al.* (1995). Litter decomposition, climate and litter quality. *Trends in Ecology & Evolution* 10, 63-66.
63. Rosenberg, N. J. *et al.* (1990). From climate and CO2 enrichment to evapotranspiration. *Climate change and US water resources.*, 151-175.
64. White, H. J. *et al.* (2020). Methods and approaches to advance soil macroecology. *Global Ecology and Biogeography* 29, 1674-1690.
65. Copernicus Climate Change Service (C3S). (ed Copernicus Climate Change Service) (2019).
66. Abatzoglou, J. T. *et al.* (2018). TerraClimate, a high-resolution global dataset of monthly climate and climatic water balance from 1958–2015. *Scientific Data* 5, 170191.
67. Speak, A. *et al.* (2020). The influence of tree traits on urban ground surface shade cooling. *Landscape and Urban Planning* 197, 103748.
68. Maclean, I. M. *et al.* (under review). On the pitfalls of measuring microclimate temperature. *Methods in Ecology and Evolution*.
69. Barnes, R. *et al.* (2017). dggridR: discrete global grids for R. *R package version 0.1.12*.
70. Wood, S. (2012). mgcv: Mixed GAM Computation Vehicle with GCV/AIC/REML smoothness estimation.
71. Stefan, V. & Levin, S. (2018). Plotbiomes: Plot Whittaker biomes with ggplot2. *R package version 0.0. 0.9001*.
72. Hengl, T. *et al.* (2017). SoilGrids250m: Global gridded soil information based on machine learning. *PLoS one* 12, e0169748.

73. Fick, S. E. & Hijmans, R. J. (2017). WorldClim 2: new 1-km spatial resolution climate surfaces for global land areas. *International Journal of Climatology* 37, 4302-4315.
74. Hall, D. K. *et al.* (2002). MODIS snow-cover products. *Remote sensing of Environment* 83, 181-194.
75. Amatulli, G. *et al.* (2018). A suite of global, cross-scale topographic variables for environmental and biodiversity modeling. *Scientific data* 5, 180040.
76. Zomer, R. J. *et al.* (2008). Climate change mitigation: A spatial analysis of global land suitability for clean development mechanism afforestation and reforestation. *Agriculture, Ecosystems & Environment* 126, 67-80.
77. Santoro, M. (2018). GlobBiomass—Global datasets of forest biomass. *PANGAEA10* 1594.
78. Dinerstein, E. *et al.* (2017). An ecoregion-based approach to protecting half the terrestrial realm. *BioScience* 67, 534-545.
79. Gorelick, N. *et al.* (2017). Google Earth Engine: Planetary-scale geospatial analysis for everyone. *Remote sensing of Environment* 202, 18-27.
80. Xu, T. & Hutchinson, M. (2011). ANUCLIM version 6.1 user guide. *The Australian National University, Fenner School of Environment and Society, Canberra*.
81. Booth, T. H. *et al.* (2014). BIOCLIM: the first species distribution modelling package, its early applications and relevance to most current MAXENT studies. *Diversity and Distributions* 20, 1-9.
82. O'Donnell, M. S. & Ignizio, D. A. (2012). Bioclimatic predictors for supporting ecological applications in the conterminous United States. *US Geological Survey Data Series* 691, 4-9.
83. Xu, Y. *et al.* (2018). Global warming will happen faster than we think. *Nature*.
84. R: a language and environment for statistical computing (R Foundation for Statistical Computing, Vienna, Austria, 2020).

Extended Data

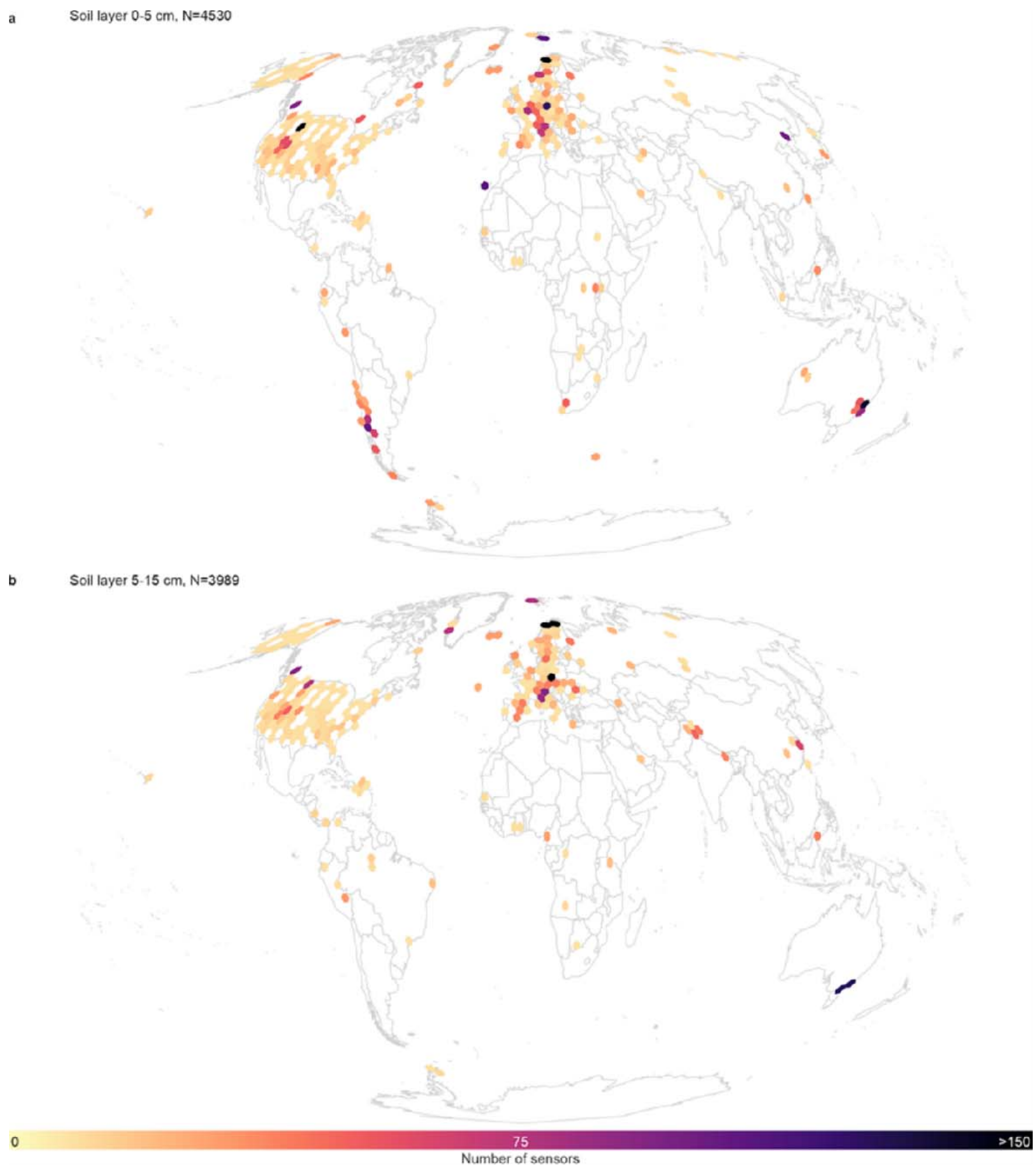

***Extended Data Figure 1: Global distribution of the in-situ measurements**. Distribution of all sensors in the topsoil (0–5 cm depth, (a), N = 4,530) and the second layer (5–15 cm depth, (b), N = 3,989). Background world map in Mollweide projection, hexagons with a resolution of approximately 70,000 km². Note that sensors appearing here and not in Fig. 1a or Extended Data Fig. 3 covered time series of less than one year, and thus were only used in the monthly models (see methods for details).*

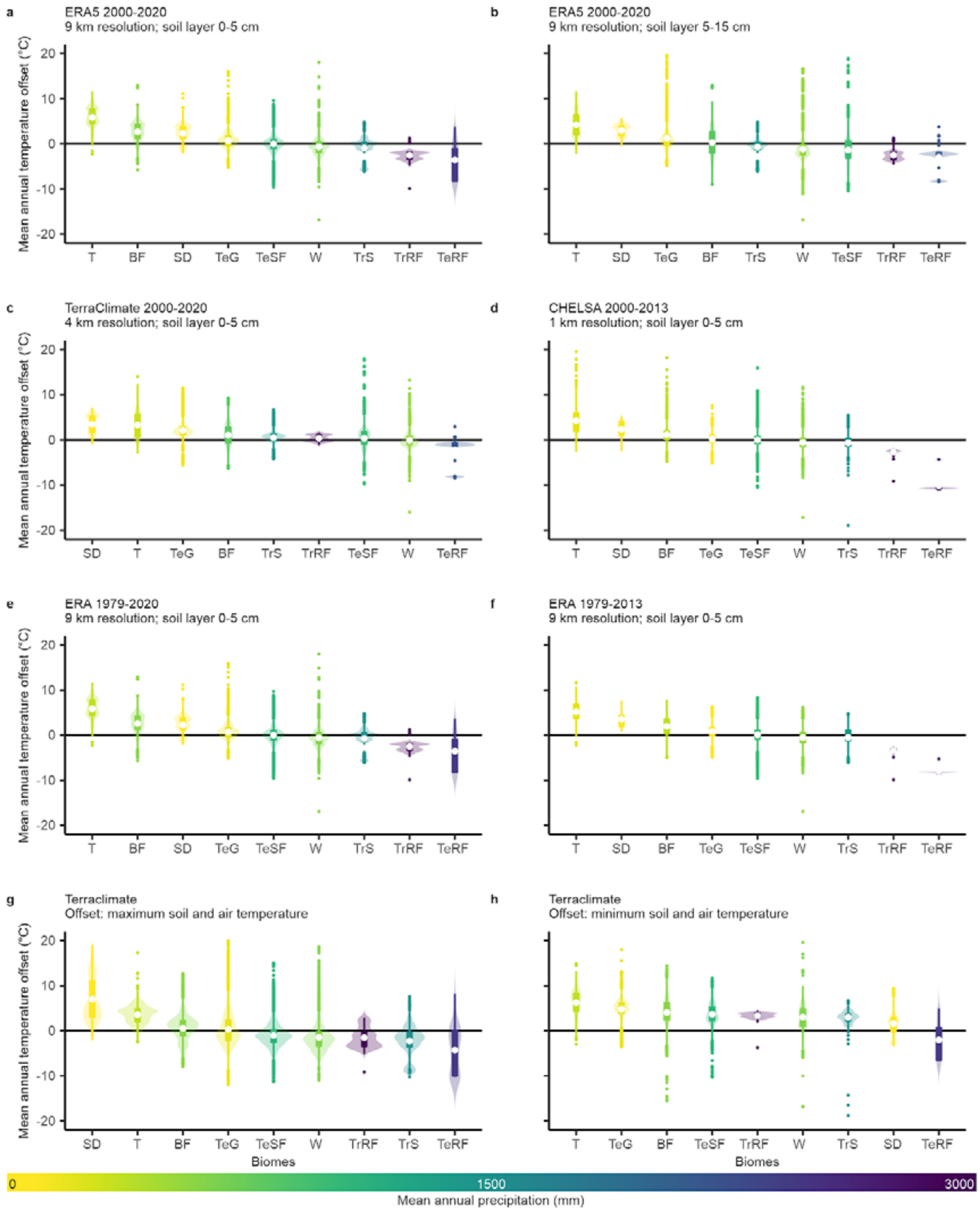

Extended Data Figure 2: Annual temperature offsets per biome *(as in Fig. 1b), for the first (0–5 cm depth) and second soil layer (5–15 cm depth) and for different air temperature data sources and time periods. Box- and violin plots of the mean annual temperature offsets per Whittaker biome, ordered and coloured by mean annual precipitation. As a standard, we used ERA5 (2000-2020, 9 km resolution) and the topsoil (0–5 cm, (a), see also Fig. 1b). We compare now with the second soil layer (5–15 cm depth, b), with TerraClimate (2000-2020, 4 km resolution, c) and CHELSA (2000-2013, 1 km resolution, d), with ERA5 for the full period (1979-2020, e) and the period matching the bioclimatic variables (1979-2013, f). We also calculate offsets between maximum (95th percentile, g) soil and air temperature, and minimum (5th percentile, h) soil and air temperature, with maximum and minimum air temperature based on TerraClimate. Panels (c) to (h) all use the topsoil data (0–5 cm depth). All* *panels show relatively consistent results (i.e. strongly positive offsets in tundra, boreal forests, subtropical deserts and temperate grasslands, and weakly negative offsets in tropical savannas and temperate and tropical rainforests). Only annual soil temperature minima were on average higher than corresponding air temperature minima in all but one biomes.*

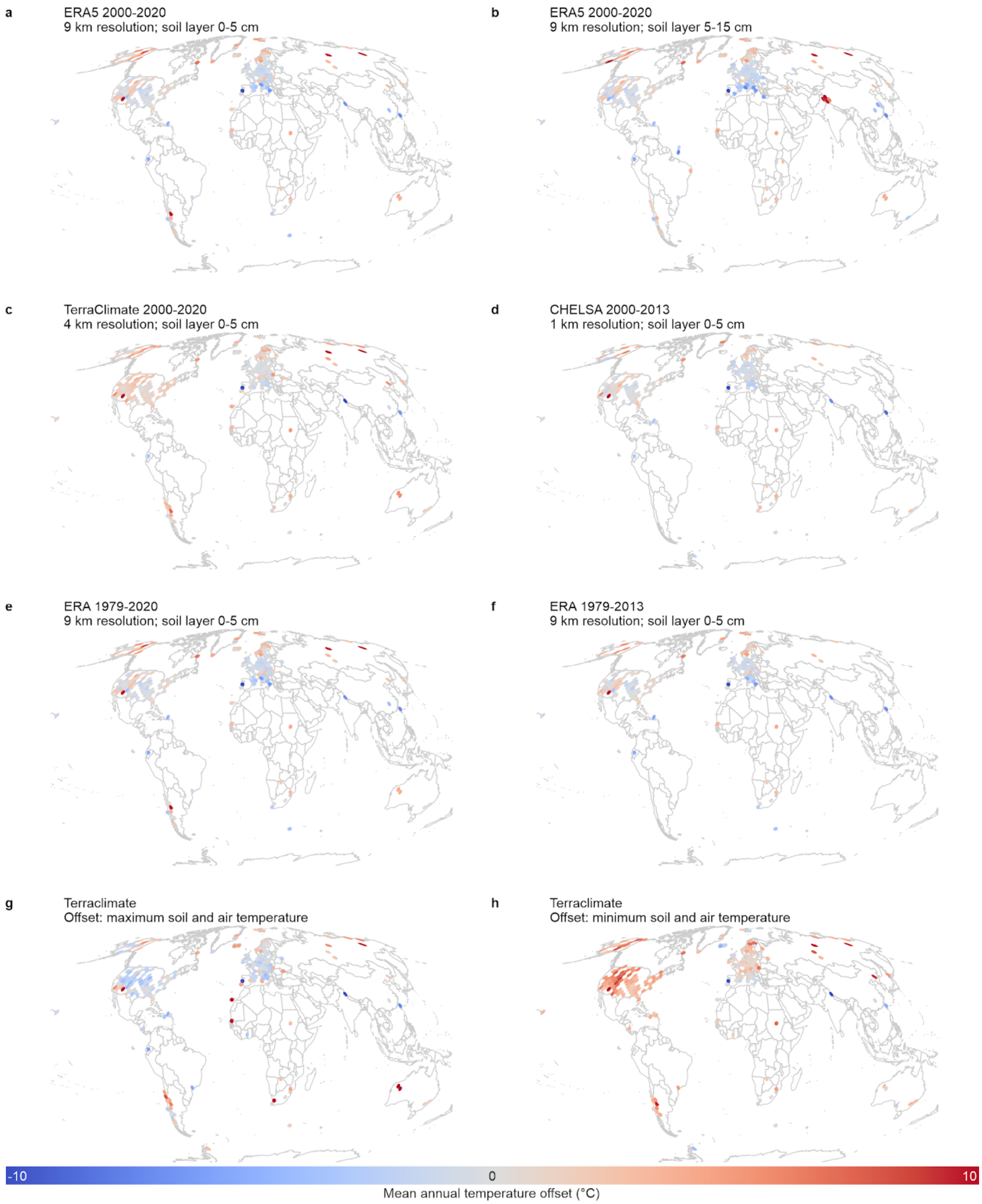

***Extended Data Figure 3: Annual temperature offset maps** (as in Fig. 1a), for the first (0–5 cm depth) and second soil layer (5–15 cm depth), for different air temperature data sources and time periods, and for maximum and minimum temperature. Distribution of sensors across the globe, coloured by the annual offset (in °C) between in-situ measured soil temperature and modelled air temperature. As a standard in Fig. 1a, we used ERA5 (2000-2020, 9 km² resolution) and the topsoil (0–5 cm, also here in a). We compare now with the second soil layer (5–15 cm depth, b), with TerraClimate (2000-2020, 4 km² resolution, c) and CHELSA (2000-2013, 1 km² resolution, d) for the topsoil layer, and with ERA5 for the full period (1979-2020,e) and the period matching the bioclimatic variables (1979-2013,* *f). We also calculate offsets between maximum (95^{th} percentile, g) soil and air temperature, and minimum (5^{th} percentile, h) soil and air temperature, with maximum and minimum air temperature based on TerraClimate. Background world map in MollWeide projection, offsets averaged per hexagon with a resolution of approximately 70,000 km^2, made using the dggridR-package in R [1]. Conclusions about consistency between methods similar as in Extended Data Fig. 2.*

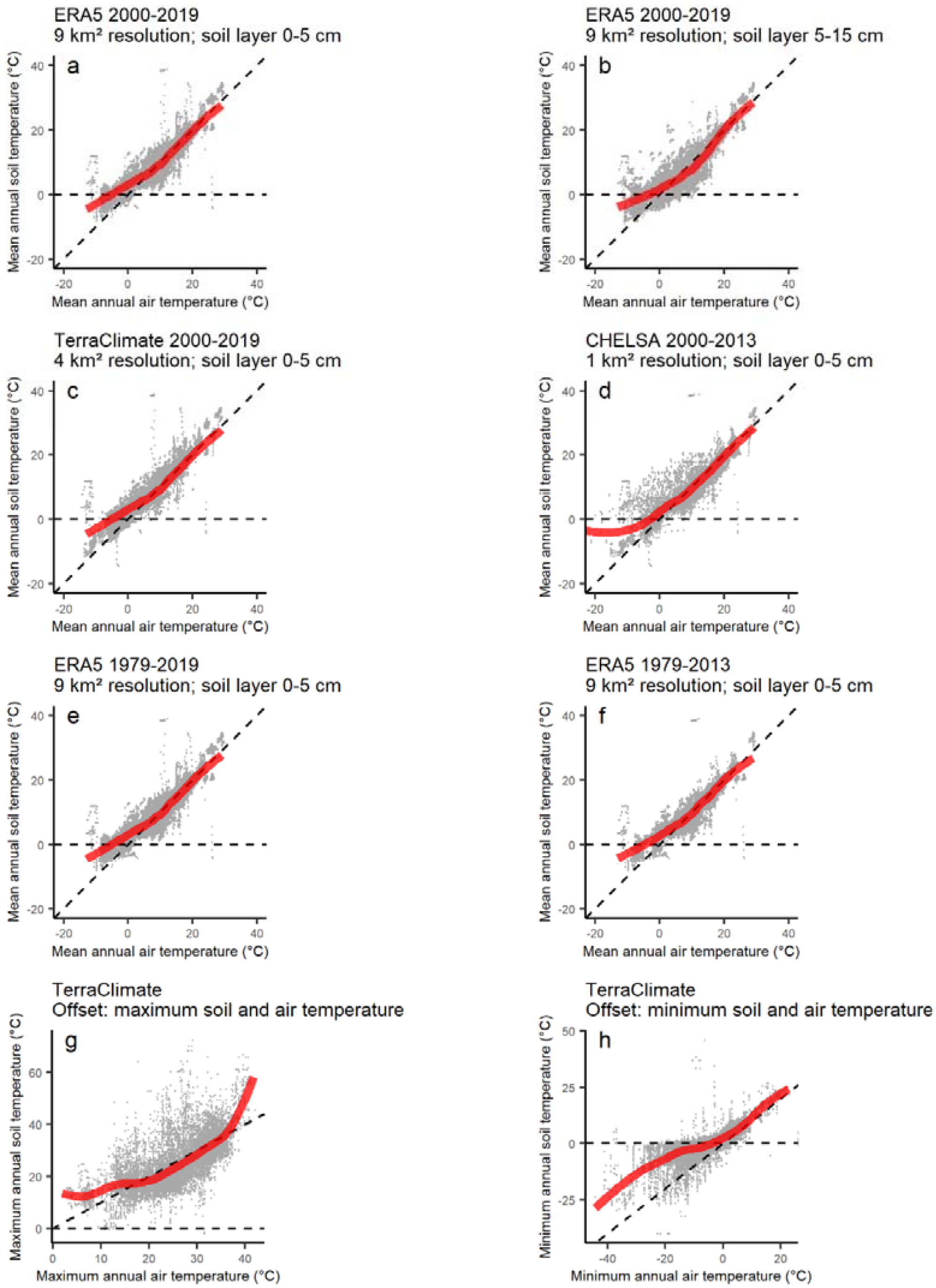

Extended Data Figure 4: Relationship between mean annual soil and air temperature at a 1 × 1 km resolution. *Point cloud of in-situ mean annual soil temperature (°C) as a function of gridded mean annual air temperature for all in-situ measurements averaged at a 1 × 1 km resolution. As a standard, we used ERA5 (2000-2020, 9 km² resolution) and the topsoil (0–5 cm depth, a). We compare this first with the second soil layer (5–15 cm depth, b). We also compare with analyses for the top soil layer using TerraClimate (2000-2020, 4 km² resolution, c) and CHELSA (2000-2013, 1 km² resolution, d), and with ERA5 for the full period (1979-2020, e) and the period matching the bioclimatic variables (1979-2013, f). We also plot offsets between maximum (95^{th} percentile, g) soil* *and air temperature, and minimum (5th percentile, h) soil and air temperature, with maximum and minimum air temperature based on TerraClimate. Straight dashed line indicate a thermal offset of 0°C, and the 1:1-relationship between soil and air temperature, thick red lines the relationship based on generalized additive models, indicating in all cases warmer soil than air temperatures in cold extremes, yet slightly cooler soils at intermediate temperatures (except for h).*

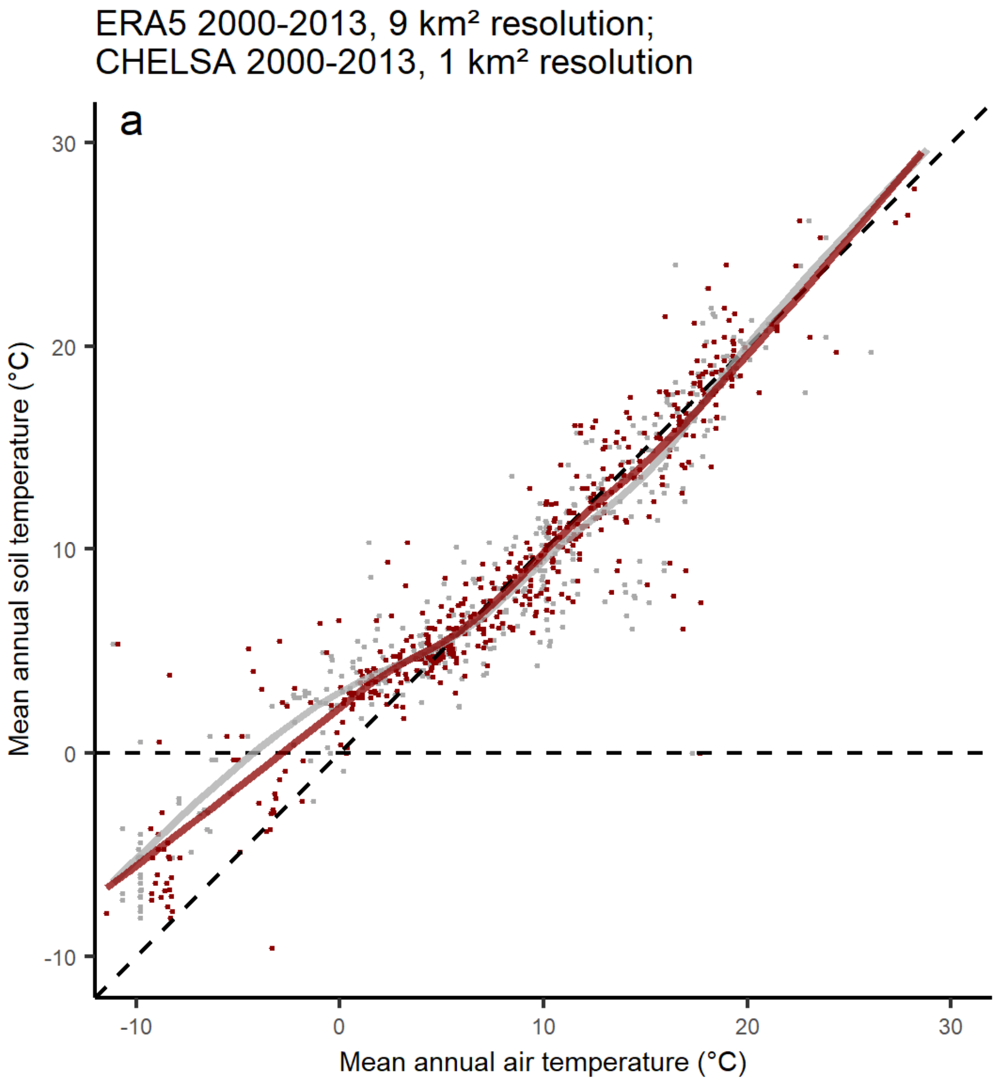

Extended Data Figure 5: Relationship between mean annual soil and air temperature for ERA5 (grey) versus CHELSA (red)*. Point cloud of in-situ mean annual soil temperature (°C) as a function of gridded mean annual air temperature for all in-situ measurements averaged at 1 km², between 2000 and 2013, for ERA5 (grey, 9-km² resolution) and CHELSA (dark red, 1 × 1 km resolution). Straight dashed line indicate a thermal offset of 0°C, and the 1:1-relationship between soil and air temperature, grey and red lines the relationship based on generalized additive models. As in Extended Data Fig. 4, yet highlighting the strong overlap in pattern when using CHELSA vs ERA5.*

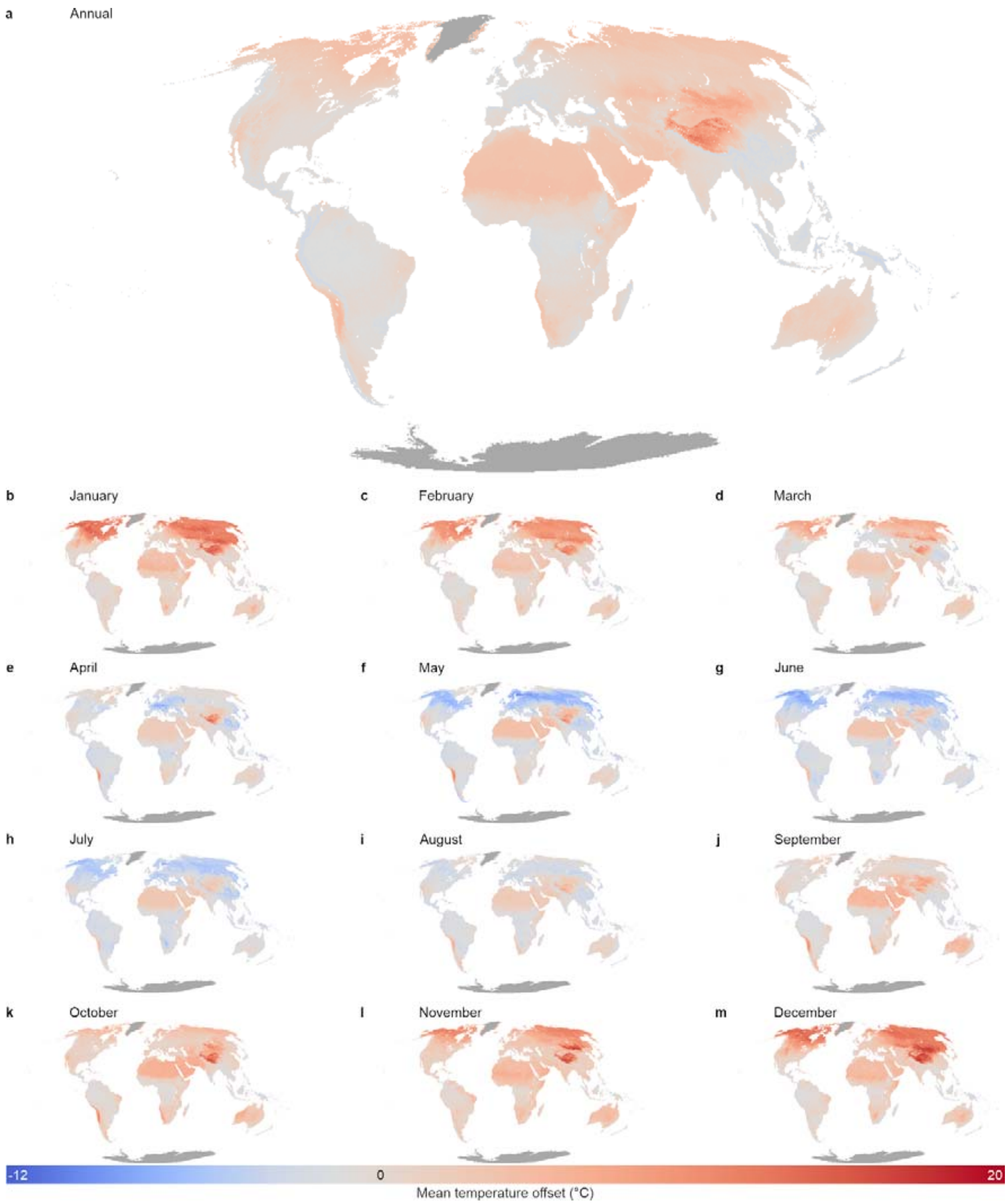

Extended Data Figure 6: Modelled mean temperature offset in the second soil layer (5–15 cm depth). *Modelled annual (a) and monthly (b-m) temperature offset (in °C) between in-situ measured soil temperature (second soil layer, 5–15 cm depth) and modelled air temperature, in addition to the first soil layer (0–5 cm depth) used in Fig. 2.*

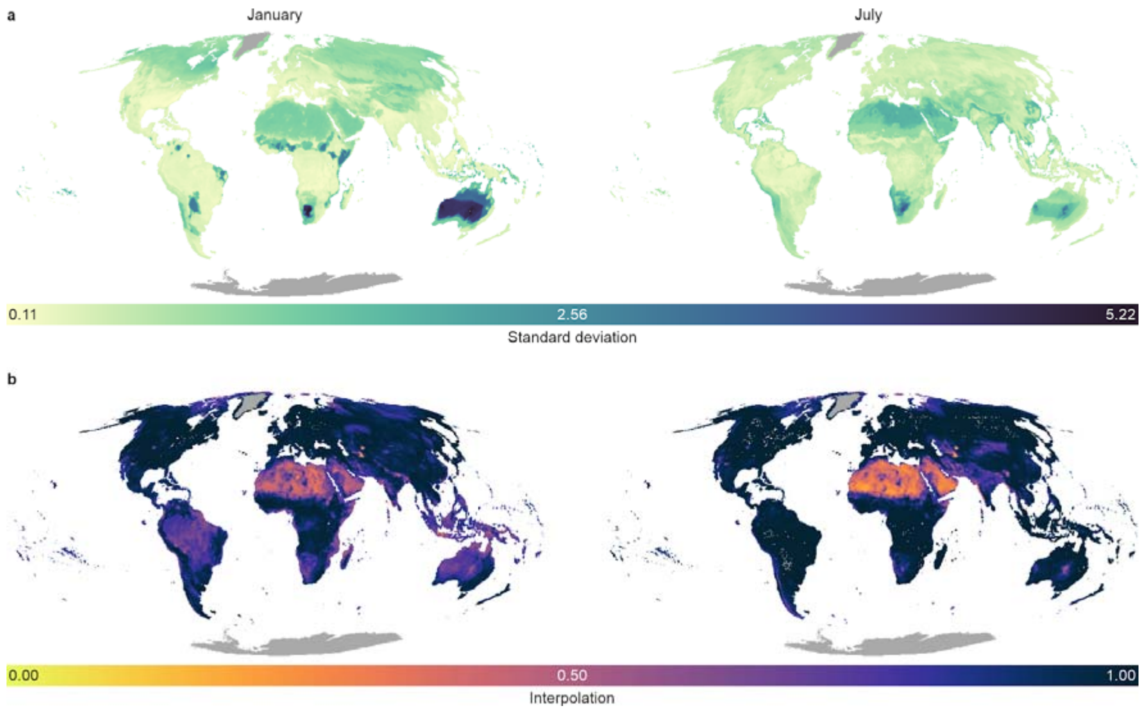

Extended Data Figure 7: Predictive performance of the temperature offset models in the second soil layer (5–15 cm depth). *Analyses for the temperature offset between in-situ second soil layer (5–15 cm depth) temperature and free-air temperature. (a) Predicted standard deviation from a cross-validation analysis that iteratively varied the set of covariates (explanatory data layers) and model hyperparameters (i.e., number of variables per split; minimum leaf population) across 100 models and evaluated model strength using 10-fold cross-validation, for January (left) and July (right), as examples of the two most contrasting months. (b) The fraction of axes in the multidimensional environmental space for which the pixel lies inside the range of data covered by the sensors in the database. Pixels with low values indicate that the model has to extrapolate for many of the environmental layers for that specific pixel.*

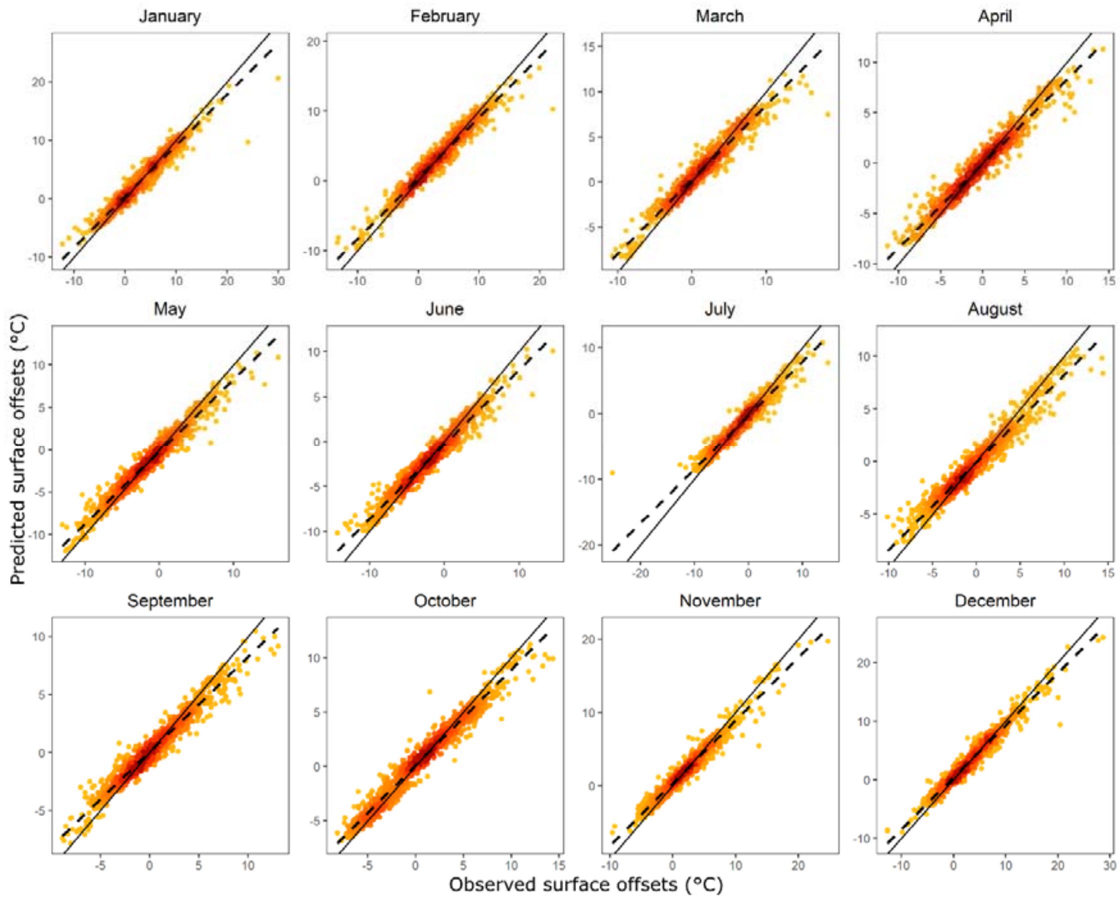

Extended Data Figure 8: Observed versus predicted temperature offsets. *Correlative plots showing temperature offsets – averaged at a 1 × 1 km resolution – as observed in the field, versus those as predicted by the models, separately for each month. Colours show density of points (darker = higher point density). Dashed lines from linear regressions; solid lines refer to the 1:1-line of perfect correlation between predicted and observed offsets.*

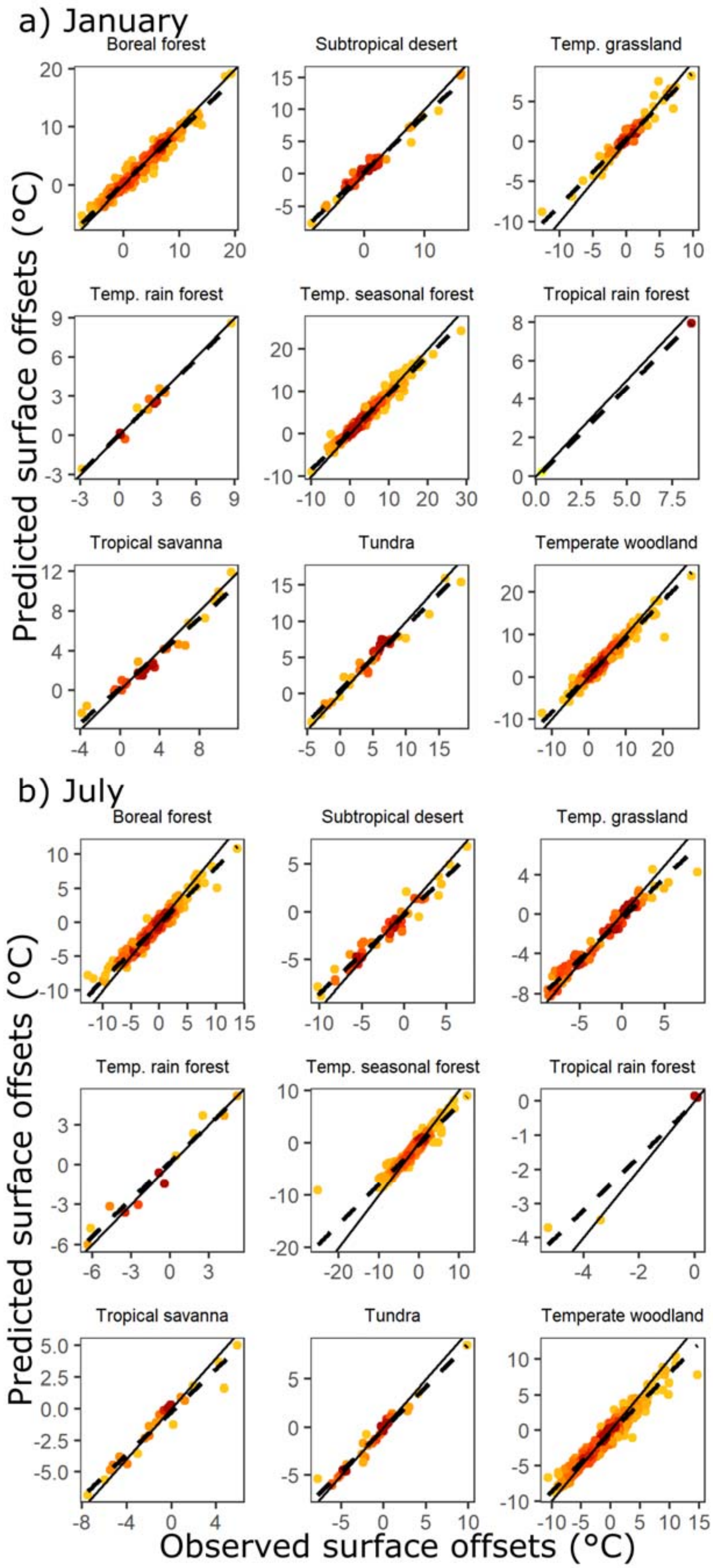

a) January
Boreal forest
Subtropical desert
Temp. grassland
Temp. rain forest
Temp. seasonal forest
Tropical rain forest
Tropical savanna
Tundra
Temperate woodland
b) July
Boreal forest
Subtropical desert
Temp. grassland
Temp. rain forest
Temp. seasonal forest
Tropical rain forest
Tropical savanna
Tundra
Temperate woodland
Predicted surface offsets (°C)
Observed surface offsets (°C)

1081

Extended Data Figure 9: Observed versus predicted temperature offsets per biome. *Correlative plots showing temperature offsets – averaged at a 1 × 1 km resolution – as observed in the field, versus those as predicted by the models, separately for each biome, for January (a) and July (b). Colours show density of points (darker = high point density). Dashed lines from linear regressions; solid lines refer to the 1:1-line of perfect correlation between predicted and observed offsets.*

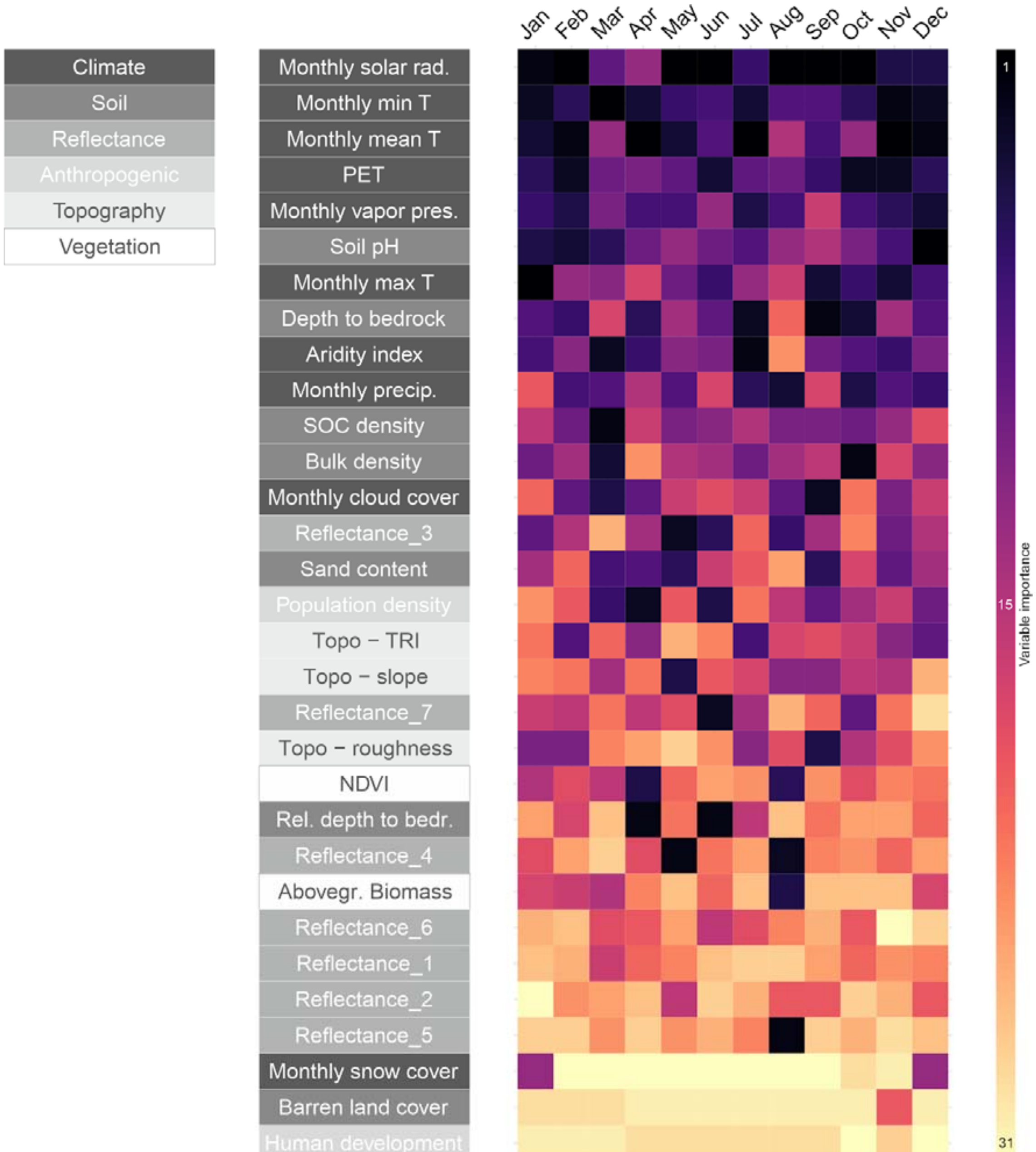

Extended Data Figure 10: Relative importance of explanatory variables. *Explanatory variables in all twelve monthly analyses sorted by mean Variable Importance (computed based on the summed decrease of impurity over all trees in the forest that results from the variable used at a node; higher for variables with a higher importance) across all models of the first soil layer (0–5 cm depth) (first variable = ranked on average most importantly across all twelve monthly models)**.** Colours represent relative variable importance (ranked from 1 to 31, with 1 the highest importance) within each monthly model for the topsoil (0–5 cm depth). T = temperature, PET = potential evapotranspiration, SOC = soil organic carbon, TRI = topographic roughness index, NDVI = normalized difference vegetation index. For full details on all explanatory variable layers, see Supplementary Table 3.*

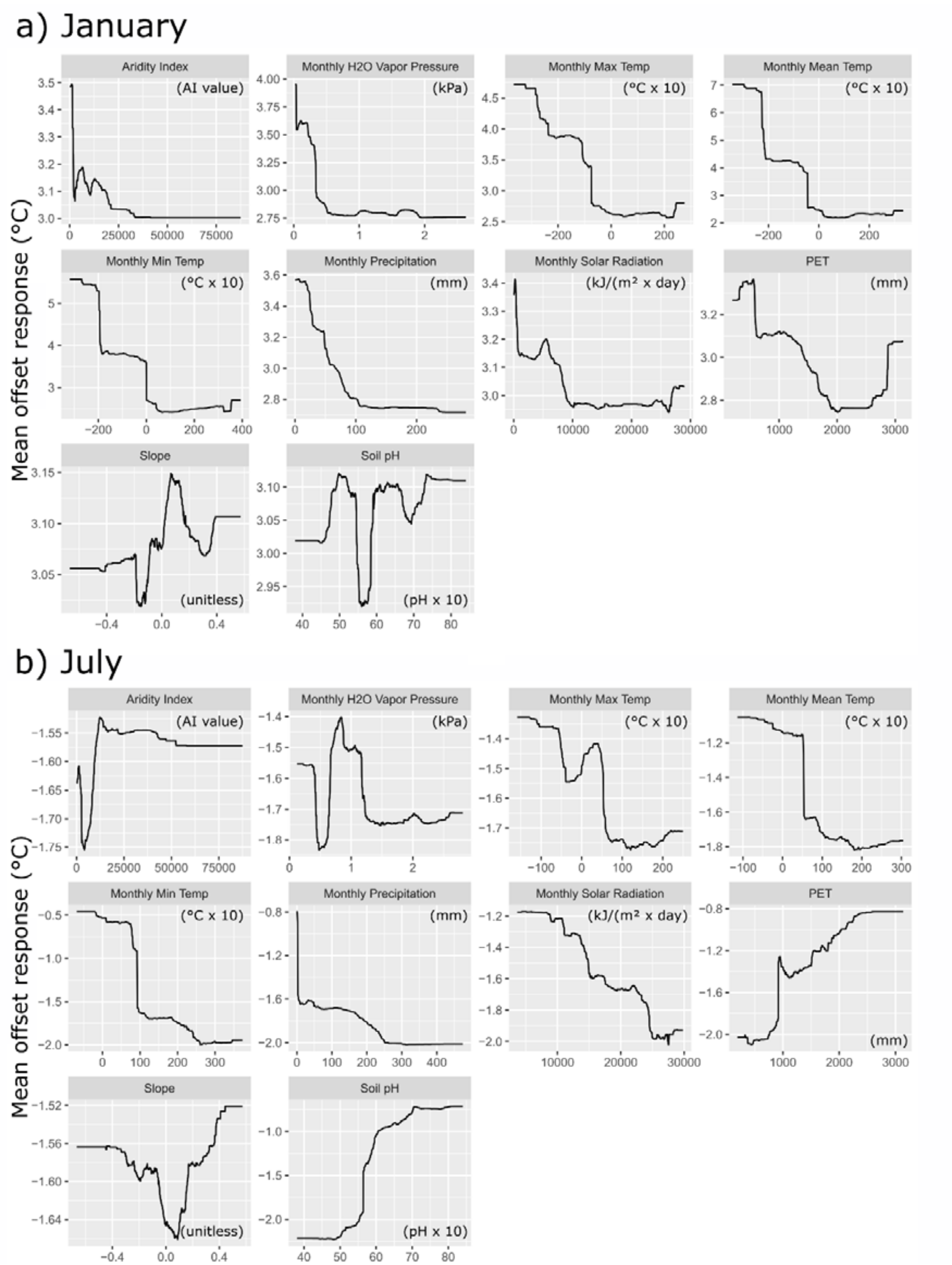

Extended Data Figure 11: Partial dependency plots of main effects. *Partial dependency plots of the 10 most important variables (selection based on the mean Feature Importance from Extended Data Fig. 10) for January (a; top) and July (b; bottom), as examples of the two most contrasting months. Results for the first soil layer (0–5 cm depth).*

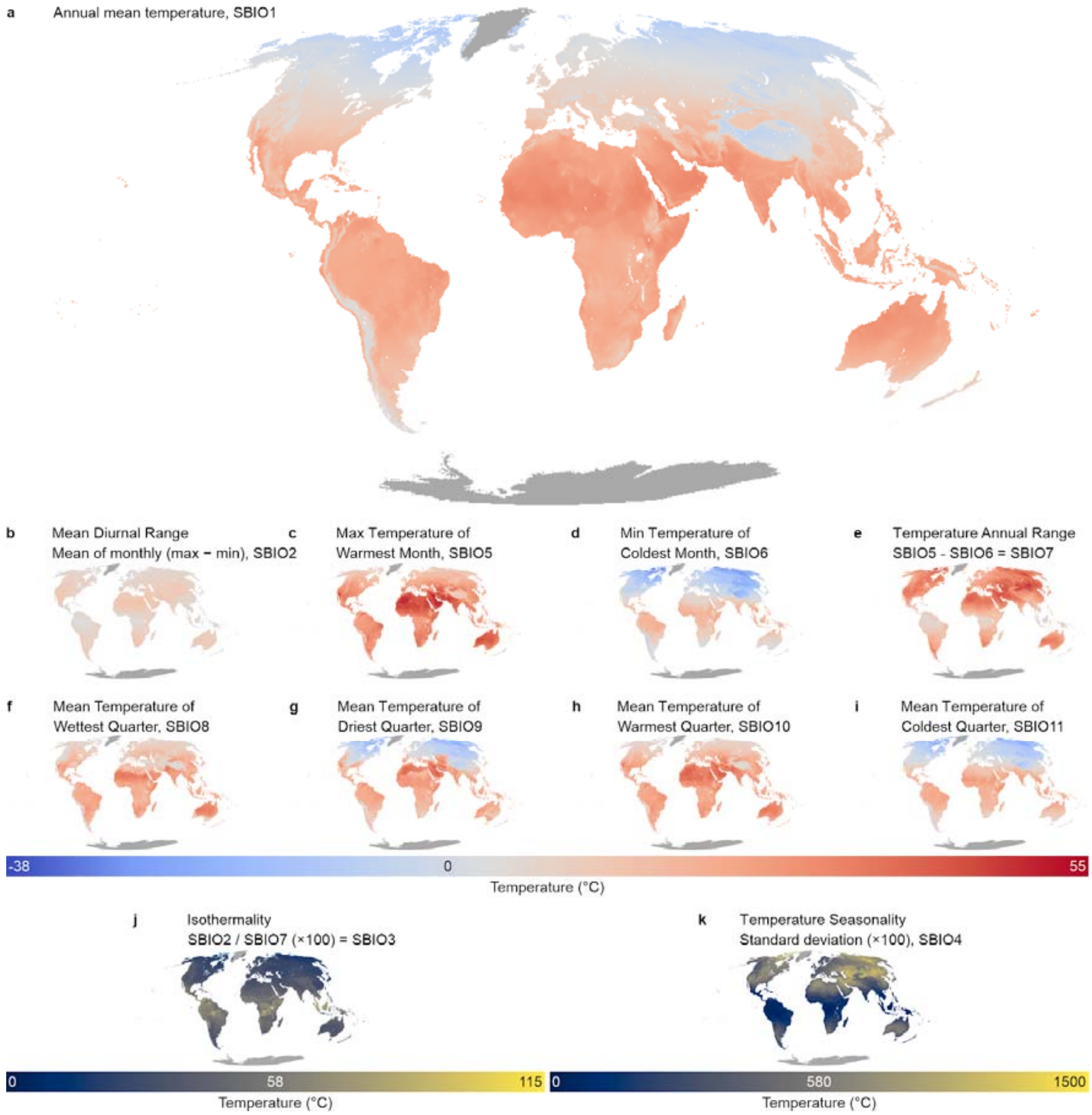

Extended Data Figure 12: Bioclimatic variables for the first soil layer. *Global maps of bioclimatic variables for topsoil (0–5 cm depth) climate, calculated using the maps of monthly soil climate (see Fig. 2, Extended Data Fig. 6), and the bioclimatic variables for air temperature from CHELSA.*

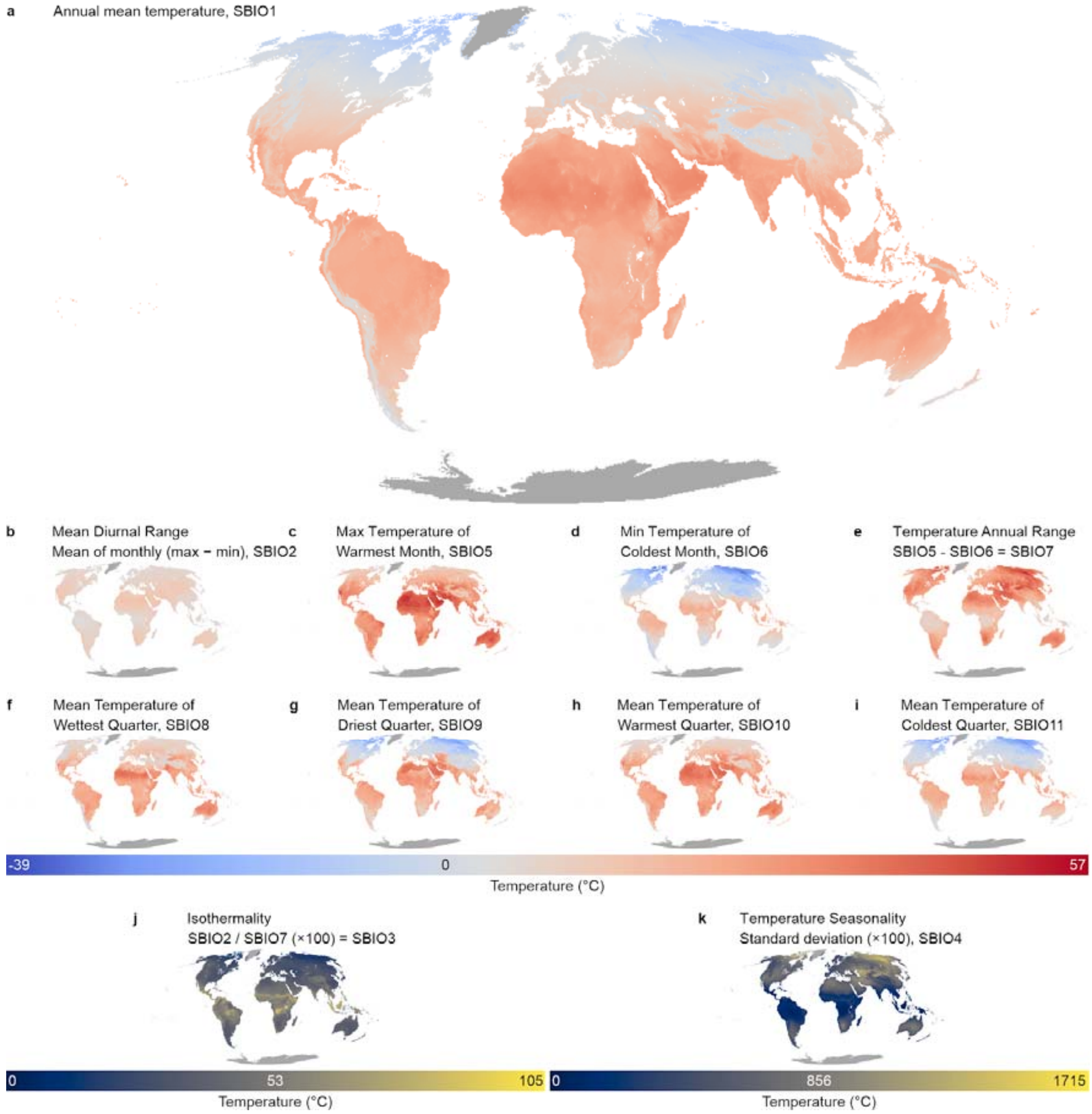

Extended Data Figure 13: Bioclimatic variables for the second soil layer. *Global maps of bioclimatic variables for the second soil layer (5–15 cm depth) climate, calculated using the maps of monthly temperature offsets (see Fig. 2, Extended Data Figure 6) and the bioclimatic variables for air temperature from CHELSA [2].*

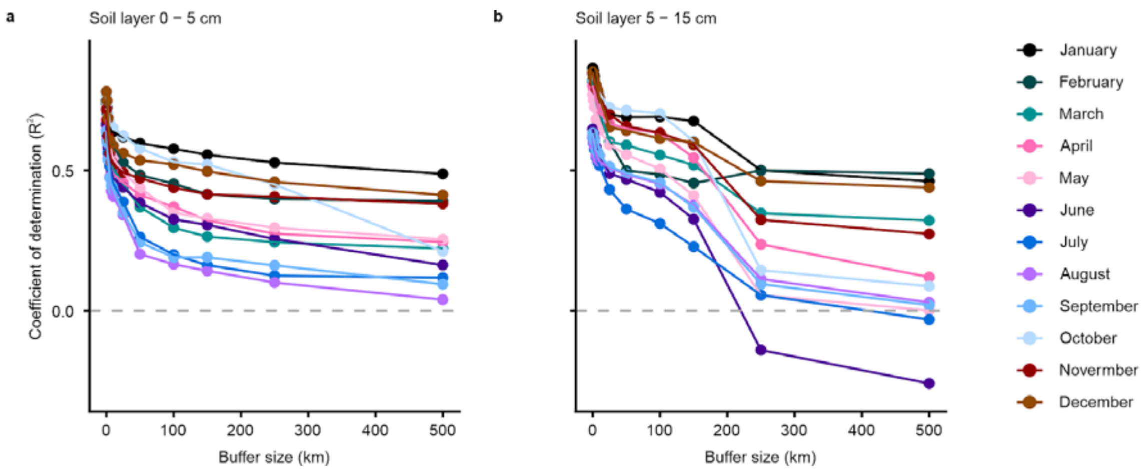

Extended Data Figure 14: spatial leave-one-out cross-validation. *R^2 of all monthly models at the two soil depths using a spatial leave-one-out cross validation approach. This approach trains a model for each sample in the dataset on all remaining samples, with an increasingly large buffer around that focal sample. Note that a decrease in R^2 should be expected with increasing buffer size due to the removal of parts of the environmental gradient from the training dataset. Nevertheless, results show that spatial autocorrelation differs across the months, with uneven global data coverage likely causing lowest confidence for May to September at 5–15 cm depth, where use of data outside of the environmental gradient as covered by the data is thus extra discouraged (see Fig 3b and Extended Data Fig. 7b).*

Extended Data Tables

Extended Data Table 1: *Number of unique pixels after averaging the annual data at 1 × 1 km pixel resolution for each biome, as used in Fig. 1. The number of individual annual averages on which this number is based is shown between brackets.*

Biome	***N° of pixels (0–5 cm)***
Boreal forest	*240 (10168)*
Sub-tropical desert	*37 (802)*
Temperate grassland	*66 (9558)*
Temperate rainforest	*10 (27)*
Temperate seasonal forest	*245 (21566)*
Tropical rainforest	*2 (299)*
Tropical savanna	*13 (2062)*
Tundra	*29 (1584)*
Temperate woodland	*224 (16952)*

Extended Data Table 2: *Difference in temperature offset between forested and unforested habitats. Mean and standard deviation of offsets per Whittaker biome for all sensors, and for sensors in forested and non-forested habitats separately. All values averaged at a 1 × 1 km resolution (number between brackets = number of unique 1 × 1 km pixels), only biomes with sufficient number of loggers in forested habitats are shown. Habitat assessment at the location of the sensor based on observations by the contributors, whenever available (60% of sensors).*

Biome	***All***	***Forested***	***Non-forested***
Boreal forest	*2.47 ± 2.01 (240)*	*3.40 ± 1.64 (41)*	*3.12 ± 1.77 (105)*
Temperate grasslands	*0.92 ± 2.13 (66)*	*1.39 ± 2.79 (4)*	*1.30 ± 2.79 (27)*
Temperate seasonal forests	*0.46 ± 2.79 (245)*	*-0.82 ± 2.21 (53)*	*1.00 ± 3.95 (20)*
Temperate woodland	*-0.12 ± 3.38 (224)*	*-0.71 ± 3.11 (31)*	*1.22 ± 4.31 (35)*

Extended Data Table 3: *Number of unique pixels after averaging the monthly data at a 1 × 1 km pixel resolution for each biome as used in the models, averaged across all months.*

Biome	***N° of pixels (0–5 cm)***	***N° of pixels (5–15 cm)***
Boreal forest	*284*	*323*
Sub-tropical desert	*46*	*4*
Temperate grassland	*82*	*63*
Temperate rainforest	*12*	*2*
Temperate seasonal forest	*349*	*304*
Tropical rainforest	*5*	*9*
Tropical savannah	*26*	*31*
Tundra	*35*	*34*
Temperate woodland	*466*	*353*

Extended Data Table 4: *Number of sensors from the most common logger brands in the top soil (left, 0–5 cm depth) and the second soil layer (right, 5–15 cm depth). Other sensors include among others Decagon devices, GeoPrecision data loggers, thermocouples and TinyTags.*

Logger brand	***Number of sensors***	
	0–5 cm	***5–15 cm***
iButton	*1840*	*1685*
TOMST	*512*	*1090*
HOBO	*689*	*491*
Lascar	*247*	*0*
Others	*1025*	*587*

Extended Data Table 5: *Number of sensors in each soil layer*

Depth of soil layer (cm)	***Number of sensors***
0–5	*4530*
5–15	*3989*
15-30	*484*
30-60	*294*
60-100	*54*
100-200	*11*

Extended Data Table 6: *Number of data points (in brackets the number of unique pixels after averaging at 1 × 1 km pixel resolution) for each month as used in the models.*

Month	***N° of data points (0–5 cm)***	***N° of data points (5–15 cm)***
January	*6674 (1212)*	*10130 (977)*
February	*6649 (1223)*	*10214 (986)*
March	*6527 (1184)*	*10345 (979)*
April	*6439 (1093)*	*10266 (989)*
May	*6611 (1150)*	*10510 (1003)*
June	*6537 (1154)*	*10546 (1011)*
July	*6874 (1352)*	*10515 (1141)*
August	*6960 (1383)*	*10950 (1098)*
September	*6690 (1317)*	*10484 (1019)*
October	*6991 (1299)*	*10429 (1018)*
November	*6995 (1215)*	*10683 (996)*
December	*6846 (1193)*	*10607 (988)*

References

1. Barnes, R. *et al.* (2017). dggridR: discrete global grids for R. *R package version 0.1.12*.

2. Karger, D. N. *et al.* (2017). Climatologies at high resolution for the earth's land surface areas. *Scientific Data* 4, 170122.

Affiliations

1) Research Group PLECO (Plants and Ecosystems), University of Antwerp, 2610 Wilrijk, Belgium, 2) Department of Environmental Systems Science, Institute of Integrative Biology, ETH Zürich, Zürich, Switzerland, 3) Finnish Meteorological Inst., P.O. Box 503, FI-00101 Helsinki, Finland, 4) Dept of Geosciences and Geography, Gustaf Hällströmin katu 2a, FIN–00014 Univ. of Helsinki, Finland, 5) Centre for Sustainable Ecosystem Solutions, School of Biological Sciences, University of Wollongong, Wollongong, Australia, 6) Australian Museum, Sydney, Australia, 7) Forest & Nature Lab, Department of Environment, Ghent University, Geraardsbergsesteenweg 267, 9090 Melle-Gontrode, Belgium, 8) Geography Research Unit, University of Oulu, Oulu, Finland, 9) Institute of Botany of the Czech Academy of Sciences, Zámek 1, CZ-25243, Průhonice, Czech Republic, 10) Faculty of Forestry and Wood Sciences, Czech University of Life Sciences Prague, Kamýcká 129, CZ-165 21, Prague 6 - Suchdol, Czech Republic, 11) Environment and Sustainability Institute, University of Exeter, Penryn Campus, Penryn, UK, TR10 9FE, 12) Department of Geography, York St John University, Lord Mayor's Walk, York, YO31 7EX, United Kingdom, 13) Department of Earth and Environmental Sciences, KU Leuven, Celestijnenlaan 200E, 3001 Leuven, Belgium, 14) School of Natural Resources and Environment, University of Florida, Gainesville, FL 32611, USA, 15) Smithsonian Environmental Research Center, Edgewater MD 21037 USA, 16) Department of Wildlife Ecology and Conservation, University of Florida, Gainesville, FL 32611, USA, 17) Department of Natural Sciences and Environmental Health, University of South-Eastern Norway, Gullbringvegen 36, NO-3800, Bø, Norway, 18) Alpine Ecosystems Research Program, Institute of Ecology, Ilia State University, Tbilisi, Georgia, 19) Department of Range Management, Faculty of Natural Resources and Marine Sciences, Tarbiat Modares University, Noor, Mazandaran Province, I. R. Iran, 20) Department of Ecological Science, Vrije Universiteit Amsterdam, The Netherlands., 21) Royal Botanic Garden Edinburgh, 20A Inverleith Row, EH3 5LR, Edinburgh, UK, 22) Environmental Science Center, Qatar University, Doha, Qatar, 23) Department of Environmental Systems Science, Institute of Integrative Biology, ETH Zurich, Universitätsstrasse 16, CH-8092 Zürich, Switzerland, 24) Research group ECOBE, University of Antwerp, 2610 Wilrijk, Belgium, 25) Department of Agroecology and Environment, Agroscope Research Institute, Reckenholzstrasse 191, 8046 Zürich, Switzerland, 26) Department of Environmental Systems Science, ETH Zurich, Universitätsstrasse 2, 8092 Zurich, Switzerland, 27) UK Centre for Ecology & Hydrology, Bush Estate, Penicuik, Midlothian, EH26 0QB, United Kingdom, 28) Department of Physical Geography and Ecosystem Science, Lund University, Sölvegatan 12, 223 62 Lund, Sweden, 29) European Commission, Joint Research Centre (JRC), Ispra, Italy, 30) Siberian Federal University, 660041 Krasnoyarsk, Russia, 31) Instituto Argentino de Nivología, Glaciología y Ciencias Ambientales (IANIGLA), CONICET, CCT-Mendoza; Facultad de Ciencias Exactas y Naturales, Universidad Nacional de Cuyo, 32) Instituto Argentino de Nivologiá, Glaciologiá y Ciencias Ambientales (IANIGLA), CONICET, CCT-Mendoza, 33) Natural History Museum, University of Oslo, 0318, Oslo, Norway, 34) Section for Ecoinformatics & Biodiversity, Department of Biology, Aarhus University, Aarhus C, Denmark, 35) Center for Biodiversity Dynamics in a Changing World, Department of Biology, Aarhus University, Aarhus C, Denmark, 36) Ecological Plant Geography, Faculty of Geography, University of Marburg, Deutschhausstrasse 10, 35032, Marburg, Germany, 37) Institute of Landscape Ecology Slovak Academy of Sciences, Štefánikova 3, 81499 Bratislava, Slovakia, 38) Faculty of Environment and Forest Sciences, Agricultural University of Iceland, Árleyni 22, 112 Reykjavík, Iceland, 39) Instituto Argentino de Nivología, Glaciología y Ciencias Ambientales (IANIGLA), CONICET, CCT-Mendoza, 40) Isotope Bioscience Laboratory - ISOFYS, Ghent University, Coupure Links 653, 9000 Gent, Belgium, 41) Université de Rennes, CNRS, EcoBio (Ecosystèmes, biodiversité, évolution) - UMR 6553, F-35000 Rennes, France, 42) Department of Sustainable Agro-ecosystems and Bioresources, Research and Innovation Centre, Fondazione Edmund Mach, Via E. Mach 1, 38010 San Michele all'Adige, Italy, 43) Forest Research, Alice Holt Lodge, Wrecclesham, Farnham, UK, 44) Department of Ecology, Pontificia Universidad Javeriana, Bogota, Colombia, 45) Jolube Consultor Botánico. C/Mariano R de Ledesma, 4. E-22700 Jaca, Huesca, SPAIN, 46) Institute of Landscape and Plant Ecology, Department of Plant Ecology, University of Hohenheim, August-von\r\nHartmann Str. 3, 70599 Stuttgart, Germany, 47) Disturbance Ecology, BayCEER, University of Bayreuth, Universitätsstr. 30, 95447 Bayreuth, Germany, 48) Norwegian Institute for Nature Research, FRAM - High North Research Centre for Climate and the Environment, P.O. Box 6606 Langnes, N-9296 Tromsø, Norway, 49) Department of Earth Sciences, University of Gothenburg, P.O. Box 460, SE-40530 Gothenburg, Sweden, 50) Gothenburg Global Biodiversity Centre, P.O. Box 461, SE-405 30 Gothenburg, Sweden, 51) Department of Biological and Environmental Sciences, University of Gothenburg, P.O. Box 461, 43 Gothenburg SE-405 30, Sweden, 52) Department of Environmental Science, Policy, and Management, University of California, Berkeley, CA 94720 USA, 53) Alfred Wegener Institute Helmholtz Center for Polar and Marine Research, Telegrafenberg A45, 14473 Potsdam, Germany, 54) Geography Department, Humboldt-Universität zu Berlin, Germany, 55) Pós-Graduação em Ciências de Florestas Tropicais, Instituto Nacional de Pesquisas da Amazônia, Manaus, Brasil, CEP: 69060-001, 56) Department of Environmental Systems Science, ETH Zurich, Universitaetstrasse 2, 8092 Zurich, Switzerland, 57) UMR ECOSYS INRAE, AgroParisTech, Uinversité Paris Saclay, France, 58) Biological Dynamics of Forest Fragments Project, BDFFP, Instituto Nacional de Pesquisas da Amazônia, Av. André Araujo, 2936 - Petrópolis, Manaus, Amazonas, 69067-375, Brazil, 59) Department of Forest Sciences, Federal University of Lavras, 37.200-900, Lavras, MG, Brazil, 60) Faculty of Arts and Sciences, Department of Molecular Biology and Genetics, Ordu University, 52200, Ordu, Turkey, 61) Department of Science and High Technology, Insubria University, Via Valleggio 11, 22100 Como, Italy, 62) Department of Chemistry, Life Sciences and Environmental Sustainability, University of Parma, Parco Area delle Scienze 11/A, 43124 Parma, Italy, 63) Department of Evolutionary Biology, Ecology and Environmental Sciences, Biodiversity Research Institute (IRBio), University of Barcelona, 08028 Barcelona, Catalonia, Spain, 64) CREAF, E08193 Bellaterra (Cerdanyola del Vallès), Catalonia, Spain, 65) Laboratorio de Ecofisiología vegetal y Cambio Climático and Núcleo de Estudios Ambientales (NEA), Universidad Católica de Temuco, Campus Luis Rivas del Canto, Rudecindo Ortega 02950, Temuco, Chile., 66) German Centre for Integrative Biodiversity Research (iDiv) Halle-Jena-Leipzig, Leipzig, Germany, 67) Institute of Biology, Leipzig University, Leipzig, Germany, 68) Laboratory of Bioclimatology, Department of Ecology and Environmental Protection, Poznan University of Life Siences, ul. Piatkowska 94, 60-649, Poznan, Poland, 69) Univ. Grenoble Alpes, Univ. Savoie Mont Blanc, CNRS, LECA, F-38000 Grenoble, France, 70) Univ. Grenoble Alpes, Univ. Savoie Mont Blanc, CNRS, LTSER Zone Atelier Alpes, F-38000 Grenoble, France, 71) School of Biological Sciences, Monash University, Victoria 3800, Australia, 72) Forest Ecology and Conservation Group, Department of Plant Sciences, University of Cambridge, Cambridge CB23EA, UK, 73) Faculty of Ecology and Environmental Sciences, Technical University in Zvolen, T. G. Masaryka 24, 960 01 Zvolen, Slovakia, 74) Sub-Antarctic Biocultural Conservation Program, Universidad de Magallanes, Pdte. Manuel Bulnes 01855, Punta Arenas, Magallanes y la Antártica Chilena, 75) Núcleo Milenio de Salmónidos Invasores, INVASAL, Concepción, Chile, 76) British Antarctic Survey, NERC, High Cross, Madingley Road, Cambridge CB3 0ET, United Kingdom, 77) Department of Arctic and Marine Biology, Faculty of Biosciences Fisheries and Economics, UiT-The Arctic University of Norway, N-9037 Tromsø, Norway, 78) Climate Change Unit, Environmental Protection Agency of

Aosta Valley, Italy, 79) Department of Biological Sciences, University of Notre Dame, Notre Dame, IN 46556, USA, 80) Department of Science, University of Roma Tre, 00146 Rome, Italy, 81) Department of Ecology, Environment and Plant Sciences and Bolin Centre for Climate Research, Stockholm University, 106 91 Stockholm, Sweden, 82) the County Administrative Board of Västra Götaland, SE-403 40 Gothenburg, Sweden, 83) School of GeoSciences, University of Edinburgh, King's Buildings, Edinburgh, EH9 3FF, United Kingdom, 84) Department of Geology, Geography and Environment. University of Alcalá. 28805 Alcalá de Henares, Madrid, Spain., 85) Institute for Alpine Environment, Eurac Research, Viale Druso 1, 39100 Bozen/Bolzano, Italy, 86) Vegetation Ecology, Institute of Natural Resource Sciences, ZHAW Zurich University of Applied Sciences, Grüental, 8820 Wädenswil, Switzerland, 87) Plant Ecology, Bayreuth Center of Ecology and Environmental Research (BayCEER), University of Bayreuth, Universitätsstr. 30, 95447 Bayreuth, Germany, 88) VITO-TAP, Boeretang 200, 2400-Mol, Belgium, 89) Swiss Federal Research Institute WSL, 8903 Birmensdorf, Switzerland, 90) Majella Seed Bank, Majella National Park, Colle Madonna, 66010 Lama dei Peligni, Italy, 91) Department of Life, Health and Environmental Sciences, University of L'Aquila, Piazzale Salvatore Tommasi 1, 67100 L'Aquila, Italy, 92) Grupo de Ecología de Poblaciones de Insectos, IFAB (INTA - CONICET), Modesta Victoria 4450, Bariloche, Argentina, 93) Faculty of Science, Department of Botany, University of South Bohemia, Na Zlaté Stoce 1, 37005 České Budějovice, Czech Republic, 94) Climate Impacts Research Centre, Department of Ecology and Environmental Sciences, Umeå University, Abisko, Sweden, 95) Global Change Research Institute, Academy of Sciences of the Czech Republic, 96) Quantitative Plant Ecology and Biodiversity Research Lab., Department of Biology, Faculty of Science, Ferdowsi University of Mashhad, Mashhad, Iran, 97) School of Biological Sciences, The University of Western Australia, Crawley, WA 6009, Australia, 98) Kings Park Science, Department of Biodiversity, Conservation & Attractions, Kings Park, 6005 WA, Australia, 99) Department of Botany, Faculty of Biology, University of Innsbruck, Sternwartestraße 15, 6020 Innsbruck, Austria, 100) Imperial College London, Silwood Park Campus, Ascot SL5 7PY, UK, 101) Operation Wallacea, Wallace House, Old Bolingbroke, Lincolnshire, PE23 4EX, UK, 102) INRAE, Bordeaux Sciences Agro, UMR 1391 ISPA, F-33140 Villenave d'Ornon, France, 103) Department of Life and Environmental Sciences, University of Cagliari, Viale Sant'Ignazio da Laconi 13, 09123, Cagliari, Italy., 104) Department of Botany, University of Granada, 18071, Granada, Spain, 105) Departamento de Biología de Organismos y Sistemas, Universidad de Oviedo, C/ Catedrático Rodrigo Uría, 33006 Oviedo/Uviéu, Spain, 106) Institute for Plant Science and Microbiology, University of Hamburg, Ohnhorststr. 18, 22609 Hamburg, Germany, 107) Dartmouth College, Hanover, NH, USA, 108) Ecosystems and Global Change Group, Department of Plant Sciences, University of Cambridge, Cambridge, CB2 3EA, United Kingdom, 109) WSL Institute for Snow and Avalanche Research SLF, 7260 Davos, Switzerland, 110) Swiss Federal Research Institute for Forest, Snow and Landscape Research WSL, 8903 Birmensdorf, Switzerland, 111) Laboratorio de Invasiones Biológicas (LIB), Facultad de Ciencias Forestales, Universidad de Concepción, Concepción, Chile, 112) School of Education and Social Sciences, Adventist University of Chile, Chile, 113) Instituto de Ecología y Biodiversidad (IEB), Santiago, Chile, 114) Pyrenean Institute of Ecology (CSIC), Av. Montañana 1005, 50059 Zaragoza, Spain, 115) Biodiversity and Landscape, TERRA research centre, Gembloux Agro-Bio Tech, University of Liège, Gembloux, 5032, Belgium ; Research Group PLECO (Plants and Ecosystems), University of Antwerp, 2610 Wilrijk, Belgium, 116) Department of Geo-information in Environmental Management, Mediterranean Agronomic Institute of Chania, PO Box 85, 73100 Chania, Greece, 117) Georgian Institute of Public Affairs, department of Environmental management ad policy, Tbilisi, Georgia, 118) Flemish Institute for Technological Research, 2400 Mol, Belgium, 119) Department of Earth and Environmental Science, Faculty of BioScience Engineering, KULeuven, Belgium, 120) Max Planck Institute for Biogeochemistry, Department of Biogeochemical Signals, Jena, Germany, 121) Sustainable Agricultural Sciences Department, Rothamsted Research, Harpenden, AL5 2JQ, UK, 122) Department of Biology, Norwegian University of Science and Technology, 7491 Trondheim, Norway, 123) Biodiversity, Wildlife and Ecosystem Health, Biomedical Sciences, University of Edinburgh, Edinburgh, EH8 9JZ, UK, 124) Department of Ecology, Swedish University of Agricultural Sciences, Box 7042, S-750 07 Uppsala, 125) School of Biological Sciences, The University of Hong Kong, Pok Fu Lam Road, Hong Kong SAR, China, 126) Department of Theoretical and Applied Sciences, Insubria University, Via Dunant 3, 21100 Varese, Italy, 127) CIRAD, UMR Eco&Sols, 34060 Montpellier, France, 128) Eco&Sols, Univ Montpellier, CIRAD, INRAE, IRD, Montpellier SupAgro, 34060 Montpellier, France, 129) Senckenberg Research Institute and Natural History Museum Frankfurt, 63571 Gelnhausen, Germany, 130) Faculty of Biology, University of Duisburg-Essen, 45141 Essen, Germany, 131) Institute of Biology / Geobotany and Botanical Garden, Martin Luther University Halle-Wittenberg, Halle (Saale), Germany, 132) Department of Biological Sciences and Bjerknes Centre for Climate Research, University of Bergen, N-5020 Bergen, Norway, 133) Centre for Biodiversity & Taxonomy, Department of Botany, University of Kashmir, Srinagar - 190006, J&K, India, 134) Department of Ecology, University of Innsbruck, 6020 Innsbruck, Austria, 135) INRAE, Univ. Bordeaux, BIOGECO, F-33610 Cestas, France, 136) TERRA Teaching and Research Center, Faculty of Gembloux Agro-Bio Tech, University of Liege, Passage des déportés, 2, 5030 Gembloux, Belgium, 137) UK Centre for Ecology & Hydrology, Penicuik, EH26 0QB, Scotland, UK., 138) Institute for Botany, University of Natural Resources and Life Sciences Vienna (BOKU), Gregor-Mendel-Straße 33/I, 1180 Vienna, Austria, 139) Centre for Agrometeorological Research (ZAMF), German Meteorological Service (DWD), Bundesallee 33, 38116 Braunschweig, Germany, 140) Dept of Biology, Memorial University, St. John's, NL, A1B 3X9. Canada, 141) Department of Biological Sciences, Simon Fraser University, Burnaby, BC, V5A 1S6, Canada, 142) Department of Geography, University of Zaragoza, Pedro Cerbuna 12, 50009 Zaragoza, Spain, 143) Plant Ecology, Albrecht-von-Haller-Institute for Plant Sciences, Georg-August University of Goettingen, Untere Karspuele 2, 37073 Goettingen, Germany, 144) Department of Bioscience and Arctic Research Centre, Grenåvej 14, 8410 Rønde, Denmark, 145) Department of Geography, Masaryk University, Faculty of Science, Kotlarska 2, 611 37, Brno, Czech Republic, 146) Department of Environmental Science, Shinshu University, Matsumoto, Japan, 147) Department of Bioscience and Arctic Research Centre, Aarhus University, Frederiksborgvej 399, 4000 Roskilde, Denmark, 148) INRAE, University of Bordeaux, BIOGECO, F-33610 Cestas, France, 149) Department of Forest Ecology and Management, Swedish University of Agricultural Sciences, 90183 Umeå, Sweden, 150) Laboratory of Meteorology, Department of Construction and Geoengineering, Faculty of Environmental Engineering and Mechanical Engineering, Poznan University of Life Siences, ul. Piatkowska 94, 60-649, Poznan, Poland, 151) Forest Research Institute, Department of Silviculture and Forest Tree Genetics, Braci Lesnej Street, No 3, Sekocin Stary, 05-090 Raszyn, Poland, 152) Bayreuth Center of Ecology and Environmental Research, 153) ARAID/IPE-CSIC, Pyrenean Institute of Ecology, Avda. de la Victoria, 16, Jaca 22700, Spain, 154) Pyrenean Institute of Ecology (IPE-CSIC), 155) Life and Environmental Sciences, University of Iceland, Sturlugata 7, 102 Reykjavík, Iceland, 156) Soil Science Department, Federal University of Viçosa, Prof. Peter Henry Rolfs Ave., 36570-900, Viçosa-MG, Brazil, 157) School of Biological Sciences, University of Bristol, Bristol, United Kingdom, 158) Biological and Environmental Sciences, Faculty of Natural Sciences, University of Stirling, Scotland, FK9 4LA, 159) Faculty of Environmental Sciences, Czech University of Life Sciences Prague, Kamýcká 129, 165 21 Prague 6 - Suchdol, Czech Republic, 160) Centre for Environmental and Climate Science, Lund University, Sölvegatan 37, 223 62, Lund, Sweden, 161) University of

Goettingen, Bioclimatology, Büsgenweg 2, 37077 Göttingen, Germany., 162) Environment Agency Austria, Spittelauer Lände 5, 1090 Vienna, Austria, 163) Centre for Ecological Research, Institute of Ecology and Botany, H-2163 Vácrátót, Alkotmány út 2-4., Hungary, 164) Experimental Plant Ecology, Institute of Botany and Landscape Ecology, University of Greifswald, D-17487 Greifswald, Germany, 165) GLORIA Coordination, Institute for Interdisciplinary Mountain Research, Austrian Academy of Sciences (ÖAW) & Department of Integrative Biology and Biodiversity Research, University of Natural Resources and Life Sciences, Vienna (BOKU), Silbergasse 30/3, 1190 Vienna, Austria, 166) Department of Arctic Biology, The University Centre in Svalbard (UNIS), 9171 Longyearbyen, Svalbard, Norway, 167) Department of Land Resources and Environmental Sciences, Montana State University, Bozeman MT, USA, 59717, 168) Climate Impacts Research Centre, Department of Ecology and Environmental Sciences, Umeå University, Vetenskapens väg 38, 98107 Abisko, Sweden, 169) Centre for Polar Ecology, Faculty of Science, University of South Bohemia, Na Zlaté Stoce 3, CZ-370 05, České Budějovice, Czech Republic, 170) Terrestrial Ecology Unit, Dept. of Biology, Ghent University, B-9000 Gent, Belgium, 171) Finnish Meteorological Institute, Climate System Research, PoB503, 00101 Helsinki, Finland, 172) INAR Institute for Atmospheric and Earth System Research/Physics, Faculty of Science, POBox 68 FI-00014 University of Helsinki, Finland, 173) Interuniversity Institute for Earth System Research, University of Granada, Granada 18006 Spain, 174) CNR Institute for Agricultural and Forestry Systems in the Mediterranean, P.le Enrico Fermi 1 - Loc. del Granatello, 80055, Portici (Napoli) Italy, 175) Faculty of Forestry, Technical University in Zvolen, T.G.Masaryka 24, 960 01 Zvolen, Slovakia, 176) CNR Insitute for Agricultural and Forestry Systems in the Mediterranean, P.le Enrico Fermi 1 - Loc. del Granatello, 80055, Portici (Napoli) Italy, 177) School of Pure & Applied Sciences, Environmental Conservation & Management Programme Open University of Cyprus, PO Box 12794, 2252 Latsia, Nicosia, 178) Department of Biology - Aquatic Biology, Aarhus University, Ole Worms Allé 1, 8000 Aarhus C, Denmark, 179) Aarhus Institute of Advanced Studies, AIAS Høegh-Guldbergs Gade 6B, 8000 Aarhus, Denmark, 180) CNR Institute of BioEconomy, Via Gobetti 101, 40129 Bologna, Italy, 181) Department of Forest Botany, Dendrology and Geobiocoenology, Faculty of Forestry and Wood Technology, Mendel University in Brno, Zemedelska 1, 613 00 Brno, Czech Republic, 182) Regional Centre for Integrated Environmental Monitoring, Odesa National I.I. Mechnikov University, 7 Mayakovskogo lane, 65082 Odesa, Ukraine, 183) Biological Dynamics of Forest Fragments Project, Coordenação de Dinâmica Ambiental, Instituto Nacional de Pesquisas da Amazônia, Manaus, AM CEP 69067-375, Brazil., 184) Swiss Federal Institute for Forest, Snow and Landscape Research (WSL), CH-8903 Birmensdorf, Switzerland., 185) Department of Biology, University of Antwerp, Universiteitsplein 1, 2610 Wilrijk, Belgium, 186) Department of Botany and Biodiversity Research Centre, University of British Columbia, Vancouver, BC, Canada, 187) Province of Antwerp, Koningin Elisabethlei 22, 2018 Antwerpen, Belgium, 188) Institute of Plant and Animal Ecology of Ural Division of Russian Academy of Science, 8 Marta st., 202, Ekaterinburg, Russia, 189) Department of Earth and Environmental Sciences, University of Pavia, Via S. Epifanio 14, Pavia, Italy, 190) Faculty of Science and Technology, Free University of Bolzano, Piazza Università 5, 39100 Bolzano, Italy, 191) Climate Change Unit, Environmental Protection Agency of Aosta Valley, Loc. La Maladière, 48, 11020 Saint-Christophe, Italy, 192) University of Freiburg, Chair of Geobotany, Schänzlestrasse 1, 79104 Freiburg, Germany, 193) Environment and Sustainability Institute, University of Exeter, Penryn Campus, Cornwall TR10 9FE, United Kingdom, 194) Centre for Ecosystem Science, School of Biological, Earth and Environmental Sciences, UNSW Sydney, NSW 2052, Sydney, Australia, 195) Department of Biology, Washington University in St. Louis, St. Louis, MO 63130, USA., 196) Department of Animal Biology, Institute of Biology, University of Campinas, Campinas, SP, CEP 13083-862, Brazil, 197) National Wildlife Research Centre, Environment and Climate Change Canada, Carleton University, 1125 Colonel by Drive, Ottawa, ON K1A 0H3, Canada, 198) Institute of Biology, Dept. of Molecular Botany, University of Hohenheim, 70599 Stuttgart, Germany, 199) Instituto de Matemática Aplicada San Luis, IMASL, CONICET and Universidad Nacional de San Luis, Ejército de los Andes 950, D5700HHW San Luis, Argentina, 200) Cátedra de Climatología Agrícola (FCA-UNER), Ruta 11, km 10, Oro Verde, Entre Ríos, Argentina, 201) Grupo de Ecología de Invasiones, INIBIOMA, CONICET/ Universidad Nacional del Comahue, Av. de los Pioneros 2350, Bariloche 8400, Argentina, 202) CSIC, Global Ecology Unit CREAF- CSIC-UAB, Bellaterra, 08193, Catalonia, Spain., 203) Mountains of the Moon University, P.O Box 837, Fort Portal, Uganda, 204) National Agricultural Research Organisation, Mbarara Zonal Agricultural Research and Development Institute, P.O Box 389, Mbarara , Uganda, 205) Department of Agroecology, Aarhus University, Blichers Allé 20, 8830 Tjele, Denmark, 206) Department of Biology, Lund University, SE-223 62 Lund, Sweden, 207) Department of Earth and Environmental Sciences, University of Pavia, Via S. Epifanio 14, 27100 Pavia, Italy, 208) Institute of Botany and Landscape Ecology, University Greifswald, D-17487 Greifswald, Germany, 209) V.N. Sukachev Institute of Forest SB RAS, Krasnoyarsk, Russia, 210) Institute of Ecology and Earth Sciences, University of Tartu, Lai 40, Tartu 51005, Estonia, 211) Section of Aquatic Biology, Department of Biology , Aarhus University, Ole Worms Allé 1, 8000 Aarhus C, Denmark, 212) Department of Biology and Ecology Center, Utah State University, 5305 Old Main Hill, Logan, UT 84322, USA, 213) Department of Life Sciences, Imperial College, Silwood Park Campus, Ascot, Berkshire SL5 7PY, UK, 214) Landscape Ecology, Institute of Terrestrial Ecosystems, Department of Environmental Systems Science, ETH Zürich, 8092 Zürich, Switzerland, 215) Unit of Land Change Science, Swiss Federal Research Institute WSL, 8903 Birmensdorf, Switzerland, 216) Department of Biology, Washington University in St. Louis, Campus Box 1137, 1 Brookings Drive, St. Louis, MO 63130 USA, 217) Department of Functional Ecology, Institute of Botany of the Czech Academy of Sciences, 37982 Třeboň, Czech Republic, 218) School of Ecology and Environment Studies, Nalanda University, Rajgir, India, 219) Department of Animal and Plant Sciences, University of Sheffield, Western Bank, Sheffield, S10 2TN, U.K., 220) CESAM & Department of Environment, University of Aveiro, 3810-193 Aveiro, Portugal, 221) Department of Agronomy, Food, Natural resources, Animals and Environment - University of Padua, 35020 Legnaro, Italy, 222) Univ. Savoie Mont Blanc, CNRS, Univ. Grenoble Alpes, EDYTEM, F-73000 Chambéry, France, 223) Universitat Autònoma de Barcelona, E08193 Bellaterra (Cerdanyola del\r\nVallès), Catalonia, Spain, 224) Department of Ecology and Biogeography, Faculty of Biological and Veterinary Sciences, Nicolaus Copernicus University, Toruń, Poland, 225) Centre for Climate Change Research, Nicolaus Copernicus University, Toruń, Poland, 226) A. Borza Botanic Garden, Babeș-Bolyai University, Cluj-Napoca, Romania, 227) Faculty of Biology and Geology, Department of Taxonomy and Ecology, Babeș-Bolyai University, Cluj-Napoca, Romania, 228) E. G. Racoviță Institute, Babeș-Bolyai University, Cluj-Napoca, Romania, 229) Centre for Sustainable Ecosystem Solutions, School of Earth, Atmospheric and Life Sciences, University of Wollongong, Wollongong, New South Wales, 2522, Australia, 230) University of Applied Sciences Trier, Environmental Campus Birkenfeld, 55761 Birkenfeld, Germany, 231) Institut Universitaire de France, 1 Rue Descartes, 75231 Paris cedex 05, France, 232) Swiss Federal Institute for Forest, Snow and Landscape Research WSL, Zuercherstrasse 111, 8903 Birmensdorf, Switzerland, 233) Aquatic Ecology & Environmental Biology, Institute for Water and Wetland Research, Faculty of Science, Radboud University Nijmegen, AJ 6525 Nijmegen, The Netherlands., 234) University of Notre Dame, Department of Biological Sciences and the Environmental Change Initiative, 235) Swiss National Park, Chastè Planta-Wildenberg, 7530 Zernez, Switzerland, 236) Remote Sensing Laboratories, Dept. of Geography, University of Zurich, Winterthurerstrasse 190, 8057 Zurich, Switzerland, 237) CIRAD, UMR Eco&Sols, BP1386, CP18524, Dakar, Senegal, 238) Eco&Sols, Univ Montpellier, CIRAD, INRAE, IRD, Institut Agro, Montpellier, France, 239) LMI IESOL, Centre IRD-ISRA de Bel Air, BP1386, CP18524, Dakar, Senegal, 240) Parc national des Ecrins - Domaine de Charance - 05000 GAP - France, 241) Universidad Nacional de San Antonio Abad del Cusco, Cusco, Perú, 242) Centro de Investigación de la Biodiversidad Wilhelm L. Johannsen, Cusco, Perú, 243) Biological Dynamics of Forest Fragments Project, PDBFF, Instituto Nacional de Pesquisas da Amazônia, Av. André Araujo, 2936 - Petrópolis, Manaus, Amazonas, 69067-375, Brazil, 244) Department of Ecology and Environmental Science, Umeå University, 901 87 Umeå, Sweden, 245) Institute of Bio- and Geosciences (IBG-3): Agrosphere, Forschungszentrum Jülich GmbH, Jülich, Germany, 246) Chair of Soil Science and Geomorphology, Department of Geosciences, University of Tuebingen, 72070 Tuebingen, Germany, 247) Department of Geography, The University of British Columbia, Vancouver, BC V6T 1Z2, 248) Department of Ecology, University of Innsbruck, Technikerstrasse 25, 6020 Innsbruck, Austria, 249) Department of Botany and Biodiversity Research, Rennweg 14, 1030 Vienna, 250) Princeton School of Public and International Affairs, Princeton University, Princeton, NJ 08540, USA, 251) Université de Lorraine, AgroParisTech, INRAE, Silva, 54000 Nancy, France., 252) Department of Soil Science and Landscape Management, Faculty of Earth Sciences and Spatial Management, Nicolaus Copernicus University, Toruń, Poland, 253) Terra Nova National Park, Parks Canada Agency, Glovertown NL, A0G3Y0, 254) Universidade Estadual do Norte Fluminense Darcy Ribeiro, Campos dos Goytacazes, Rio de Janeiro, Brazil, 255) National Forest Centre, Forest Research Institute Zvolen, T. G. Masaryka 22, 96001 Zvolen, Slovakia, 256) Asian School of Environment, Nanyang Technological University, 42 Nanyang Ave, Singapore 639815, Singapore, 257) Department of Geography, University of British Columbia, 1984 West Mall, Vancouver, BC V6T 1Z2, 258) Department of Earth and Environmental Sciences, Celestijnenlaan 200E, 3001 Leuven, Belgium, 259) Universidade Federal da Paraíba, Departamento de Geociências. Cidade Universitária, João Pessoa - PB, CEP 58051-900, Brasil, 260) Goethe-Universität Frankfurt, Department of Physical Geography, Altenhöferallee 1, 60438 Frankfurt am Main, Germany, 261) Department of Evolution, Ecology, and Organismal Biology, University of California Riverside, Riverside, CA, 92521, USA, 262) Department of Natural History, NTNU University Museum, Norwegian University of Science and Technology, NO-7491 Trondheim Norway, 263) UR 'Ecologie et Dynamique des Systèmes Anthropisées' (EDYSAN, UMR 7058 CNRS-UPJV), Univ. de Picardie Jules Verne, Amiens, France, 264) EnvixLab, Dipartimento di Bioscienze e Territorio, Università degli Studi del Molise, Via Duca degli Abruzzi s.n.c., 86039 Termoli, Italy, 265) Institute of Meteorology and Climate Research (IMK), Department of Atmospheric Environmental Reserach (IFU), Karlsruhe Institute of Technology (KIT), Kreuzeckbahn Straße 19, 82467 Garmisch-Partenkirchen, Germany\r\n, 266) Swedish University of Agricultural Sciences, Swedish Species Information Centre, Almas allé 8 E, 75651 Uppsala, Sweden, 267) University Duisburg-Essen, Faculty for Biology, Universitätsstr. 5, 45141 Essen, Germany, 268) Department of Geosciences and Natural Resource Management, University of Copenhagen, Øster Voldgade 10, DK-1350 Copenhagen, Denmark , 269) Experimental Plant Ecology, Institute of Botany and Landscape Ecology, University of Greifswald, partner in the Greifswald Mire Centre, D-17487 Greifswald, Germany, 270) Fondation J.-M. Aubert, 1938 Champex-Lac, Switzerland, 271) Département de Botanique et Biologie végétale, Université de Genève, Case postale 71, CH-1292 Chambésy, Switzerland, 272) Department of Geography and Earth Sciences, Aberystwyth University, Wales, UK, 273) Plant Ecology Group, Department of Evolution and Ecology, University of Tübingen, Auf der Morgenstelle 5, 72076 Tübingen, Germany, 274) Center for Systematic Biology, Biodiversity and Bioresources - 3B, Babeș-Bolyai University, Cluj-Napoca, Romania, 275) Northern Environmental Geoscience Laboratory, Department of Geography and Planning, Queen's University, 276) Graduate School of Life and Environmental Sciences, Osaka Prefecture University, 599-8531, Japan, 277) Nature Research Centre, Akademijos 2, 08412 Vilnius, Lithuania, 278) Institute of Biological Research Cluj-Napoca, National Institute of Research and Development for Biological Sciences, Bucharest, Romania, 279) CNR Institute for BioEconomy, Via Giovanni Caproni, 50144 Firenze, Italy, 280) The Ecosystem Management Research Group (ECOBE), University of Antwerp, 2610 Wilrijk (Antwerpen), Belgium, 281) Plant Conservation and Population Biology, Department of Biology, KU Leuven, Kasteelpark Arenberg 31, 3001 Heverlee, Belgium, 282) A.N. Severtsov Institute of Ecology and Evolution, Russian Academy of Sciences, 119071, Leninsky pr.33, Moscow, Russia, 283) Netherlands Institute of Ecology, Droevendaalsesteeg 10, 6708 PB, Wageningen, 284) Plant Ecology & Nature Conservation Group Wageningen University , Droevendaalse Steeg 3a 6708 PB Wageningen, 285) Centre for Integrative Ecology, School of Life and Environmental Sciences, Deakin University, Burwood, Victoria, Australia, 3125, 286) CAVElab - Computational and Applied Vegetation Ecology, Department of Environment, Ghent University, Coupure Links 653, 9000 Gent, Belgium, 287) Earth Surface Processes Team, Centre for Environmental and Marine Studies (CESAM), Dept. Environment and Planning, University of Aveiro, 3810-193, Aveiro, Portugal, 288) Instituto Pirenaico de Ecología, IPE-CSIC. Av. de la Victoria, 16. 22700 Jaca (Huesca) Spain, 289) CNR - Institute for Agricultural and Forestry Systems in the Mediterranean, P.le Enrico Fermi 1- Loc. del Granatello, 80055, Portici, (Napoli), Italy, 290) Institute of Earth Surface Dynamics, Faculty of Geosciences and Environment, University of Lausanne, Géopolis, 1015 Lausanne, Switzerland, 291) Forest Research, Northern Research Station, Roslin, EH25 9SY, UK, 292) Institute of Mountain Hazards and Environment, Chinese Academy of Sciences, Chengdu, P.R. China, 293) Department of Earth and Environmental Sciences, Lehigh University, Bethlehem, PA 18015, United States, 294) Institute for Peat and Mire Research, School of Geographical Sciences, Northeast Normal University, Changchun, Jilin 130024, China, 295) High Meadows Environmental Institute, Princeton University, NJ 08544, USA, 296) Zhejiang Tiantong Forest Ecosystem National Observation and Research Station, School of Ecological and Environmental Sciences, East China Normal University, Shanghai 200241, China, 297) JJL received funding from the National Natural Science Foundation of China (grant nr. 32071538), 298) University of Bayreuth, Ecological-Botanical Gardens, Universitaetsstr. 30, Bayreuth, Germany, 299) Key Laboratory of Geographical Processes and Ecological Security in Changbai Mountains, Ministry of Education, School of Geographical Sciences, Northeast Normal University, Changchun 130024, China